The impact of gustiness on sea surface height in storm surge situations

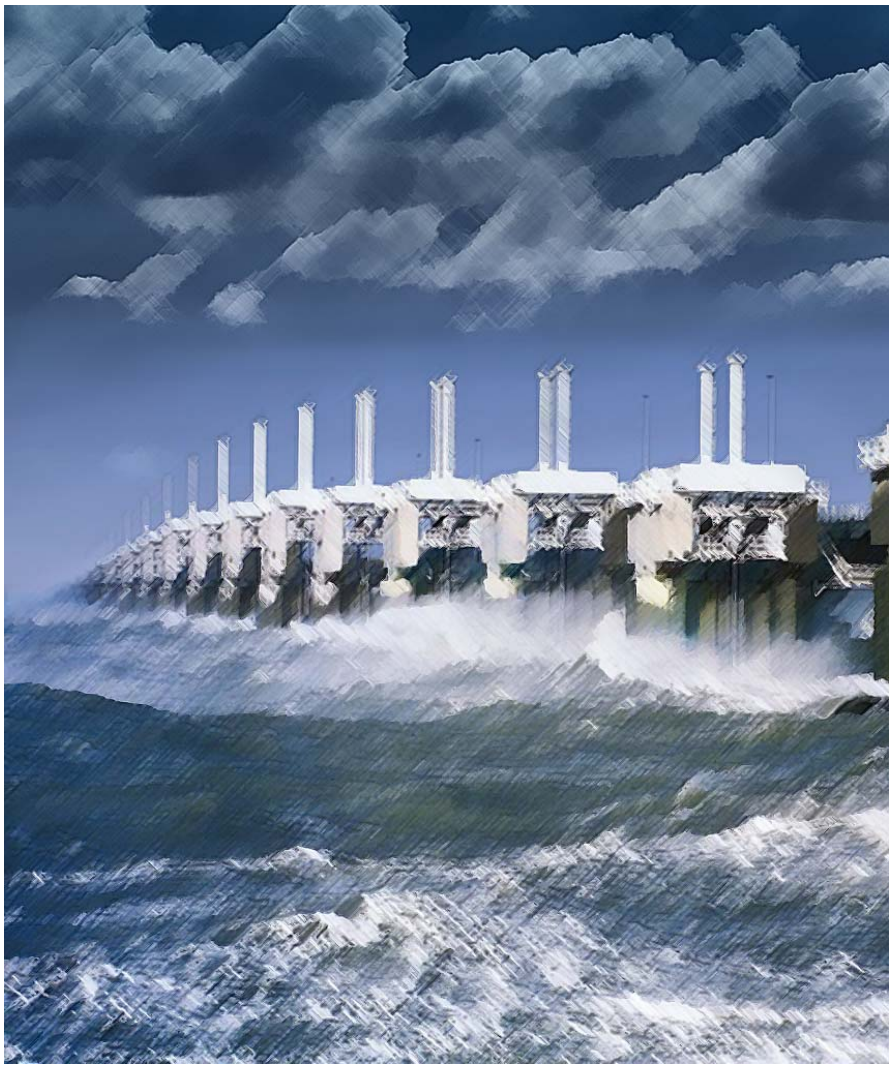

Masters Thesis
Rikke van der Grinten
Meteorology, Physical Oceanography and Climate
IMAU, University Utrecht

Supervisor IMAU
Huib de Swart

Supervisor KNMI
Hans de Vries

April 7, 2011

Abstract

In this study the influence of wind gusts on sea surface height in storm surge situations is investigated. The storm surge model WAQUA/DCSM is used for this purpose. Gustiness was modelled in Monte Carlo experiments of idealised uniform wind fields. It is concluded that high gustiness amplifies a storm surge. This is due to the non-linear behaviour of the drag relation that defines the amount of surface stress on the water.

A parameterisation for the effect that is found in the Monte Carlo experiments is presented and verified with a non-uniform wind field. The parameterisation was used in the model (called new model). In this way a model with implicit gustiness (traditional model) and explicit addition of gustiness (new model) could be compared.

With ECMWF fields of wind, pressure and wind gust (only for in the new model) sea surface heights were simulated for the storm surge season 2007 - 2008. The results of the simulations of the new model were compared with those of the traditional model and observations of gauges along the Dutch coast. The new model deviates from the traditional model in high storm surge cases.

In a statistical analysis of the two models and the observations, we found that there is no clear correlation between the error of WAQUA/DCSM and the addition in surge due to gustiness. Furthermore, the range of the error of WAQUA/DCSM is far larger than the addition due to gustiness. It is thus concluded that for the moment it is not important to include explicit gustiness in the WAQUA/DCSM model. When large errors in WAQUA/DCSM are diminished, it can become more necessary.

Contents

Chapter 1

Introduction

A storm surge is an abnormal off shore rise of water due to high wind stress and low pressure. The stress that is exerted on the sea surface due to the wind generates movement of the water. At some locations it piles up and at others it is moved away. We define a storm surge as the height of the observed sea level (also called storm tide) minus the height of the predicted tide (also called astronomical tide). This is shown in Figure 1.1. The skew surge is defined as the local maximum (or minimum) of the sea level minus the local maximum (or minimum) of the astronomical tide.

Storm surges can have enormous consequences and risks, like flooding of areas adjacent to seas and oceans. Buildings and nature are heavily damaged and societies are seriously disrupted. Tropical cyclones are a much studied extreme weather event related to storm surges. Hurricane Katrina in 2005 was an example of a cyclone, where, besides the damage that is caused by strong winds, the surge that was generated in the ocean had tremendous consequences [Knabb et al., 2005]. It had a landfall near the highly populated area of New Orleans, Louisiana. Most of the 1833 fatalities were caused by the storm surge-induced flooding. About 80% of the city of New Orleans was flooded at this event. Other examples of locations that are vulnerable for hurricane induced storm surges are the coasts on the Bay of Bengal or the Philippines.

Also at higher latitudes storm surges occur. The North Sea coasts have always been subject to the risk of flooding due to surges generated by heavy storms. The Netherlands and Great Britain have experienced several of these severe floods throughout history. At times it caused thousands of casualties [Brooks and Glasspoole, 1928]. The most recent big flooding in the south-western part of the Netherlands occurred on 1 February 1953.

Since knowledge about storm surges is so important to society, the subject has been studied thoroughly. Examples are the 'avant la lettre' numerical computations of surges along the Dutch coast by Hendrik Lorentz in the 1920's. This was related to the building of a closure dike in the Zuiderzee. One of the key motives to build a closure dike in the Zuiderzee was to prevent storm surges in North Holland. However, a serious point of investigation of the scientific Committee Lorentz was to assess the effect of the dam on surges and tides along the coasts of Wadden islands and Friesland. The results led to a relocation of the dike that decreased the risk of flooding of the Dutch coast [Lorentz, 1926].

In the second half of the 20^{th} century, several numerical models have been developed to further investigate and predict storm surges. Most of these models use non-linear depth averaged shallow water equations. Due to the introduction of these models, knowledge about storm surges has increased enormously. Mechanisms behind storm surges are understood better. Storm surges can be predicted relatively accurately.

For the prediction of storm surges, a major problem are uncertainties in the meteorological models. Storm surge models are forced by wind and pressure fields. In operational use, these fields are produced by atmospherical models. If there are errors in these fields, they are transferred into errors in surge height along the coast. Paths of low pressure areas, especially cyclones, are hard to predict precisely. Several statistical, assimilation and super-ensemble methods can be used to improve the prediction of paths of cyclones, [Vijaya Kumar et al., 2007, Madsen and Jakobsen, 2004].

An aspect that has not been studied much in this context is the influence of the short term variability of the wind. It has been suggested that the surge is enhanced in cases with very high gustiness [Koopmann, 1962]. Cavaleri and Burgers investigated the consequences of wind gustiness on the growth of wind waves

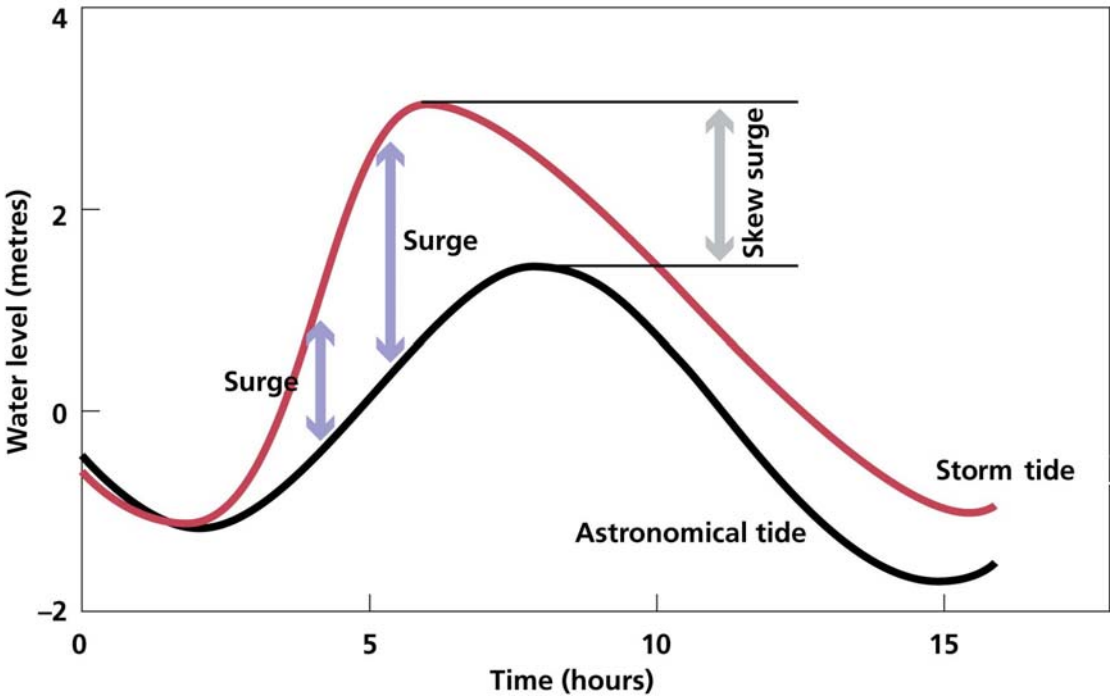

Figure 1.1: Sketch of a time series of the sea level (storm tide), astronomical tide, surge and skew surge. After UKCP09 [2010].

[Cavaleri and Burgers, 1992]. They found that that growth rate and wave energy are affected by short term wind variability. Wave energy was increased for high values of gustiness. Analogous to its effect on waves, we expect an effect of short term wind fluctuations on storm surges. In this study we will investigate this more thoroughly, and we investigate the importance of this effect relative to other errors that are introduced in storm surge forecasting.

Traditionally, storm surge models such as WAQUA/DCSM[1], are driven with hourly wind and pressure fields produced by atmospheric models, e.g. HiRLAM[2]. These wind fields are interpolated in time, but shorter time variations are not taken into account. This is depicted in a sketch in Figure 1.2, which shows a time series of observed wind speed. Short term variations are recognised. The red line denotes what would be the input of for a storm surge model, by using only interpolated hourly winds. Much information on short time scales is not taken into account.

The stress that is exerted on the sea surface by the wind is computed from the wind velocity via the drag relation. As will be shown in section 2.1.2, this relation is non-linear. This non-linear behaviour is becoming important when short term fluctuations in the wind are considered. When we take the time average over these fluctuations, they will not add up to zero, but result in a positive value. In other words: the mean stress is increased by the addition of short term fluctuations.

One has to keep in mind that the mean effect of the short term variations is already taken into account in storm surge models. This is due to the tuning of the models. In the drag relation the Charnock coefficient is tuned, when the model is calibrated for a certain domain. It is used to optimise the correspondence of the observations and model outcomes. In this way a mean contribution due to short term variations is already in the model. But from situation to situation the amount of the short term fluctuations can vary. So the contribution of the short term variations to the stress on the sea surface may also vary.

[1]Dutch Continental Shelf Model (WAQUA/DCSM) is a numerical storm surge model of the North Sea. It has been developed by Rijkswaterstaat and KNMI. It uses non-linear shallow water equations and is based on the WAQUA software package [Gerritsen et al., 1995].

[2]High Resolution Limited Area Model, an operational forecast model for the atmosphere of western Europe.

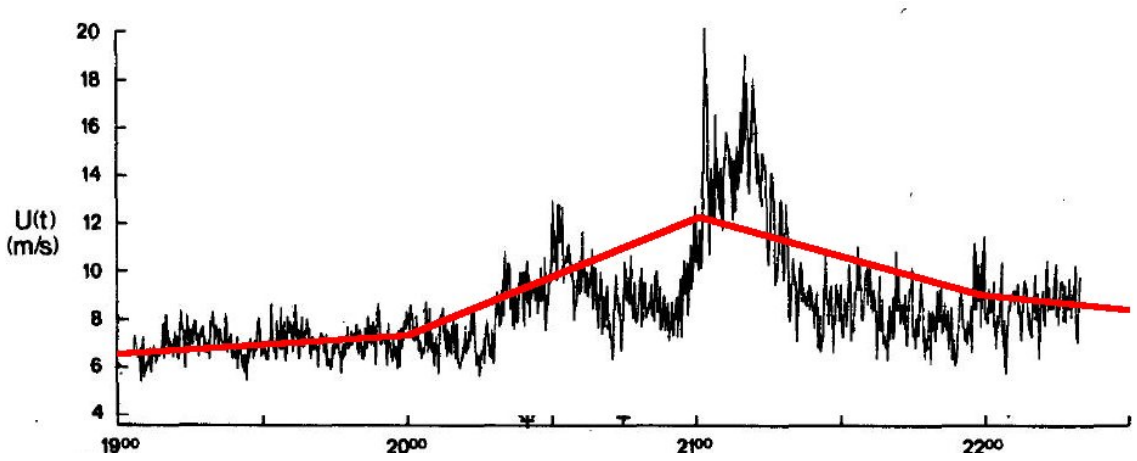

Figure 1.2: Sketch of a time series of observed wind speed (black) and the input for WAQUA/DCSM when using hourly wind (red). Figure based on Beljaars [1987]

Our key question will be: Can part of the error of the storm surge model be explained by the varying effect of short term fluctuations? How big is this part of the error, when we add the effect of short term fluctuations explicitly to the model, compared to other errors that are introduced in the system, e.g. by errors in atmospherical input and errors in bathymetry?

As a measure for the amount of short term fluctuations, we will use the term *gustiness*, which we define as the standard deviation of the (longitudinal) short term fluctuations. This term should not be confused with a term that is related to it, *wind gust*, which is the maximum of the wind in a prescribed time interval. This is an output parameter of atmospheric models like ECMWF or HiRLAM. In this study, we will deduce the gustiness from the wind gust (see section 2.2.2).

The answer to the questions will be given at the end of this study. It is done by statistically comparing predictions of a model with inclusion of varying gustiness (New model) and predictions of the old model without inclusion of gustiness (Traditional model) to sea level measurements along the Dutch coast (Observations).

But before we can use the new model in the statistical comparison, the new model first has to be developed. To investigate the exact effect of varying gustiness on the storm surge, we designed experiments with simple idealised wind fields. Random variations are added to slowly varying uniform wind fields to model short term wind fluctuations, and sensitivity experiments are performed. In this way the effect of gustiness can be studied precisely in controlled situations (see chapter 3).

But in a new model, we do not want to add random variations to model short term fluctuations. From the results of the idealised sensitivity experiments we extract a parameterisation for varying gustiness in the new model. The parameterisation is presented in section 3.6. With this new model it is also possible to look at realistic situations with variation of gustiness, slowly varying wind and pressure in time and space. ECMWF fields of wind, pressure and wind gust are used as input for some case studies of severe storms in the North Sea in 2007. The traditional and new model are compared for these cases in sections 4.1 and 4.2. Also observations of water levels were available for comparison.

Finally, in sections 4.3 and 4.4 results are presented and analysed of a long run with the old and new model for the whole storm season September 2007 to April 2008. High and low waters are compared to observations in a statistical way. This was done for five stations along the Dutch coast: Vlissingen, Hoek van Holland, Den Helder, Harlingen, Delfzijl. The error that can (not) be explained by inclusion of varying gustiness is compared to the general error of WAQUA/DCSM. In chapters 5 and 6 the study is finished with a discussion of the results and conclusions.

Chapter 2

Theory and Models

2.1 Theory

2.1.1 Storm Surges

As was explained in the introduction, a storm surge is defined as an abnormal increase of the sea level, relative to the predicted tide, associated with high velocity winds and low pressure systems.Figure 2.1 reveals that the time scale T of storm surges is relatively long, in the order of days. This means that the Coriolis effect is important ($fT \sim 1$). Also the length scale L of a storm surge wave is relatively long. In the North Sea for instance this is a in the order of a few hundreds of kilometres. When comparing it to the typical depth H of the North Sea, 50 meters, an assumption of $H \ll L$ is reasonable. Hence shallow water theory can be used. Upon making the additional assumptions that the fluid is homogeneous and inviscid, the simplified depth averaged 2-dimensional shallow water equations read [Vreugdenhil, 1994]

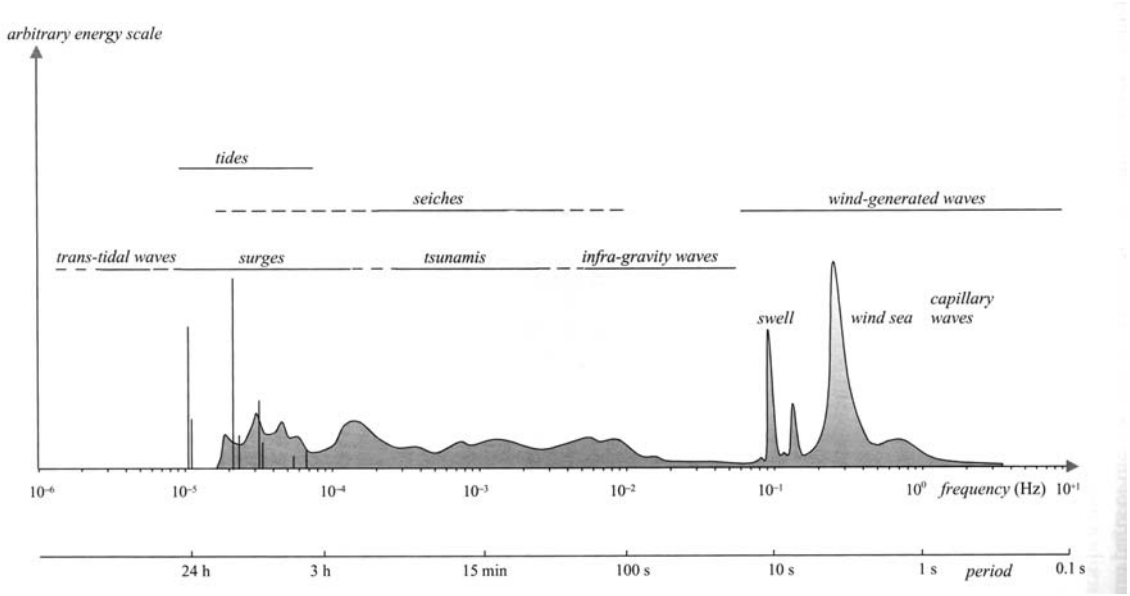

Figure 2.1: Energy spectrum of sea surface variations. After Holthuijsen [2007].

$$\frac{\partial hu}{\partial t} + \frac{\partial hu^2}{\partial x} + \frac{\partial huv}{\partial y} - fhv + gh\frac{\partial \zeta}{\partial x} - \frac{\tau_{b_x}}{\rho} = \frac{\tau_{s_x}}{\rho} + \frac{\partial p_a}{\partial x} \tag{2.1}$$

$$\frac{\partial hv}{\partial t} + \frac{\partial huv}{\partial x} + \frac{\partial hv^2}{\partial y} + fhu + gh\frac{\partial \zeta}{\partial u} - \frac{\tau_{b_y}}{\rho} = \frac{\tau_{s_y}}{\rho} + \frac{\partial p_a}{\partial y} \tag{2.2}$$

$$\frac{\partial \zeta}{\partial t} + \frac{\partial hu}{\partial x} + \frac{\partial hv}{\partial y} = 0, \tag{2.3}$$

with surface stress and bottom stress

$$\begin{aligned} \boldsymbol{\tau_s} &= \begin{pmatrix} \tau_{s_x} \\ \tau_{s_y} \end{pmatrix} = \rho_a C_d \|\boldsymbol{u_a}\| \boldsymbol{u_a} \\ \boldsymbol{\tau_b} &= \begin{pmatrix} \tau_{b_x} \\ \tau_{b_y} \end{pmatrix} = \frac{\rho g}{C^2} \|\boldsymbol{u}\| \boldsymbol{u}. \end{aligned} \tag{2.4}$$

Here,

x, y	horizontal coordinates,
t	time,
$\boldsymbol{u}$	depth mean velocity,
u, v	depth mean velocity components of fluid,
ζ	sea surface elevation with respect to mean sea level,
H	depth below mean sea level,
h	total depth of fluid, $h = \zeta + H$,
g	gravitational acceleration,
f	Coriolis parameter,
$\boldsymbol{\tau_s}$, $\boldsymbol{\tau_b}$	surface stress and bottom stress,
τ_{s_x}, τ_{s_y}	components of surface stress,
τ_{b_x}, τ_{b_y}	components of bottom stress,
p_a	atmospheric pressure
ρ, ρ_a	density water, density air,
C_d	air-sea drag coefficient,
$\boldsymbol{u_a}$	wind velocity,
C	Chézy bottom friction parameter.

These shallow water equations are generally used in storm surge modelling. As conditions on the boundaries of the domain often are taken: no orthogonal flow at closed boundaries; the sea level of astronomical tides imposed at the open boundaries.

Often these models are forced by water levels of tides at the open boundaries and by wind stress and pressure from meteorological models. Further, the condition of no orthogonal flow at a closed boundary is imposed.

Local solution

To find out more about the properties of a surge wave in a basin like the North Sea, we simplify the situation for now. We follow the simple approach of Gill [1982] on storm surges along an open coastline. The coast is taken along the x-axis, with a shallow sea in the positive y-direction. We assume no variations in the x-direction. The bottom stress is neglected. At $t = 0$ a wind stress is applied on the water surface in the

positive x-direction. After linearisation the equations (2.1) - (2.3) become

$$\begin{aligned} \frac{\partial u}{\partial t} - fv &= \frac{\tau_{s_x}}{\rho H} \\ \frac{\partial v}{\partial t} + fu &= -g\frac{\partial \zeta}{\partial y} \\ \frac{\partial \zeta}{\partial t} + H\frac{\partial v}{\partial y} &= 0. \end{aligned} \tag{2.5}$$

Boundary conditions read: $v = 0$ at $y = 0$ and the flow is bounded, i.e. does not go to infinity. A solution of v can be expressed in a steady part and a transient part. A qualitative image of the steady-v solution is given in Figure 2.2. The wind blows along the coast in the positive x-direction. This initiates an Ekman flow that is directed towards the coast. This Ekman flow is constant in time. As a consequence, the sea level rises towards the coast. The shape of the sea surface is exponential in the y-direction. The changing pressure gradient (normal to the coast) due to the change of the sea surface is in geostrophic equilibrium with a strengthening current u parallel to the coast. This effect is found on the scale of the Rossby radius of deformation.

Next to a steady solution for v, also a transient solution exists. This solution has properties that include a wave front that moves out of the coast with shallow water gravity wave speed. After $t \approx f^{-1}$ the solution near the coast will be dominated by the solution of the steady part.

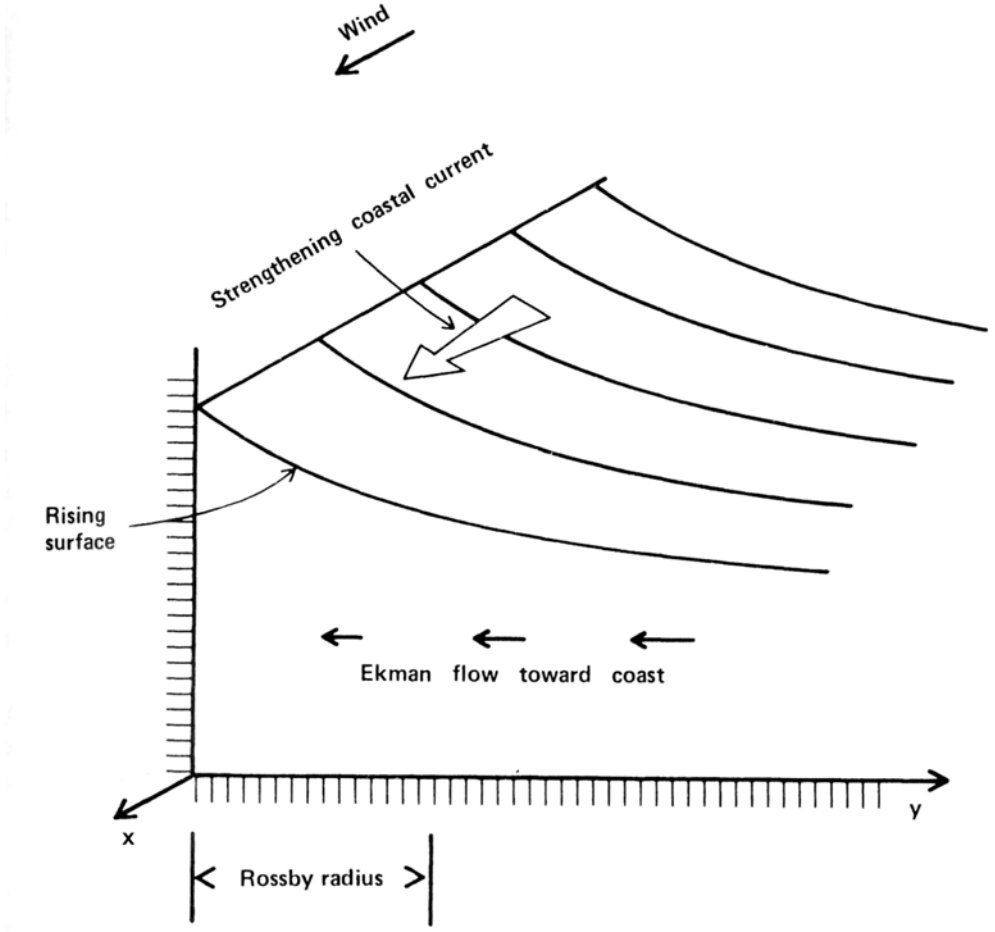

Figure 2.2: Local solution of the linearised shallow water equations, with no variation allowed in the x-direction. After Gill [1982].

Kelvin Wave

Gill [1982] also discusses a second model, that explains the wave behaviour of many observed storm surges. Contrary to the local solution, that is shown before, variations in the x-direction are allowed. But we assume that the long-shore scale is larger compared with the cross shore scale, which has a length scale in the order of the Rossby radius of deformation. After linearisation, a solution of a Kelvin wave is obtained (Figure 2.3). The sea level increases towards the coast and the wave propagates along the coast with the coast on the right hand side on the Northern Hemisphere. The propagation speed of a Kelvin wave is the same as for shallow water gravity waves: $c = \sqrt{gH}$. The Kelvin wave is modified by the wind. For an observer travelling at Kelvin-wave speed this ocurrs in the same way as in the local solution. Wind causes Ekman transport, the sea level is adjusted, and this causes an along shore flow. This is how the amplitude of the Kelvin wave can be adjusted.

In these two examples the governing equations are much simplified. It shows us the physical characteristics of a storm surge. However, geometrical details, friction, cross-shore wind stress, inverse barometer effect, wave set-up and non-linear interaction also influence storm surges. In numerical models these effects, or some of these effects, are taken into account. They adjust the appearance of the surge. Computations with numerical models provide reasonably good predictions of a storm surge if accurate meteorological input is used.

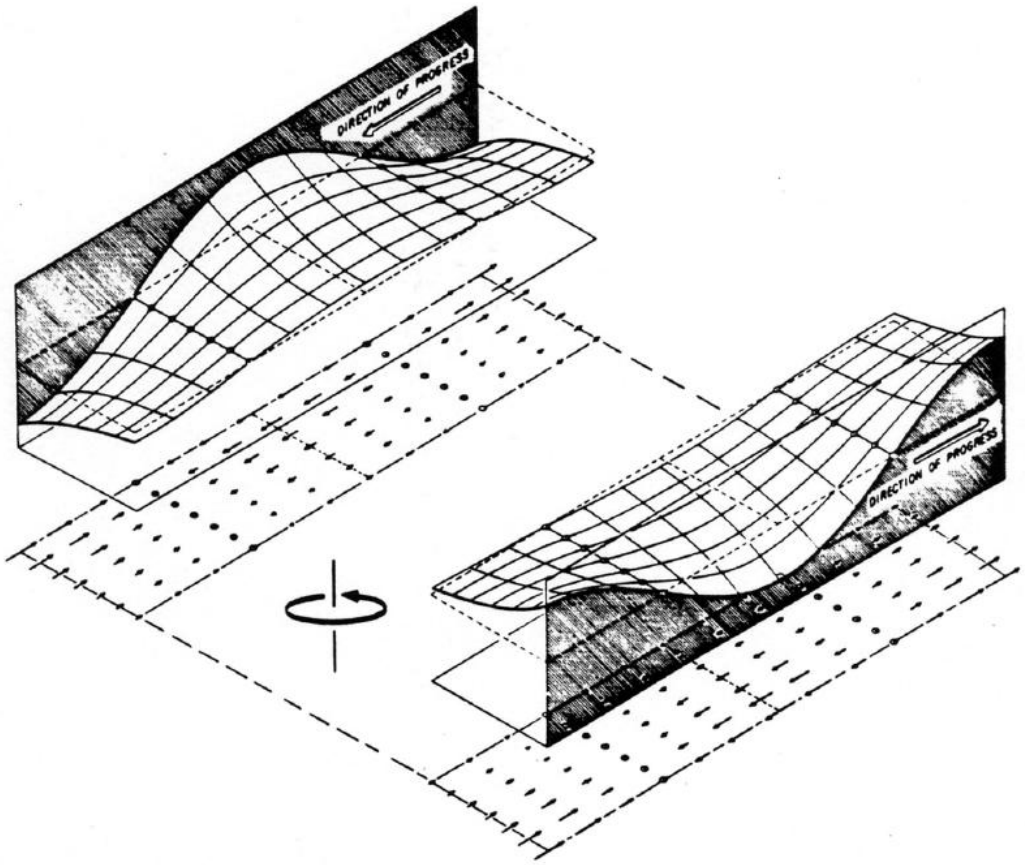

Figure 2.3: Northern Hemisphere Kelvin waves on opposite sides of a channel that is wide compared to the Rossby radius. In each vertical plane parallel to the coast, the currents are shown by arrows. The waves move with the coast on their right on the Northern Hemisphere and on the left on the Southern Hemisphere. After Gill [1982].

2.1.2 Short term fluctuations of the wind

From the storm surge wave itself we now move to the wind forcing on the surface of the water. Traditionally, operational storm surge models are forced with hourly wind fields created by atmospheric models. In reality, shorter term wind fluctuations are present in the lowest part of the atmosphere. These short term motions occur in complicated irregular patterns, both in space and time. They can be described in statistical terms [Tennekes and Lumley, 1972, Garratt, 1992].

To examine the influence of these short term effects on a storm surge, we take a closer look at the air-sea interaction. The stress that drives the system at the air-water interface can be expressed as a quadratic function of the horizontal wind velocity and also points in the direction of the wind, thus [Gill, 1982]

$$\boldsymbol{\tau_s} = C_d \rho_a \|\boldsymbol{u_a}\| \boldsymbol{u_a}. \tag{2.6}$$

Here, $\boldsymbol{\tau_s}$ is the stress, ρ_a is the air density and $\boldsymbol{u_a}$ is the wind vector at 10 m height. Furthermore, C_d is the drag coefficient, a bulk parameter, which depends on atmospheric conditions and wave state. For neutral conditions it is described by the Charnock relation [Charnock, 1955]

$$\begin{aligned} C_d &= \frac{u_\star^2}{\|\boldsymbol{u_a}\|^2}, \quad \text{with} \\ u_\star^2 &= \frac{\|\boldsymbol{\tau_s}\|}{\rho_a} \\ \frac{\|\boldsymbol{u_a}\|}{u_\star} &= \frac{1}{\kappa} \ln(\frac{gz}{u_\star^2}) - \ln \beta_C. \end{aligned} \tag{2.7}$$

Here, $u_\star$ represents the friction velocity, z is a reference height above mean sea level, here $z = 10$m. Furthermore, κ is the Von Karman constant and g is the gravitational velocity. In the last term β_C is the Charnock coefficient [Geernaert, 1999]. In numerical storm surge models the Charnock coefficient is used as a tuning parameter [Onvlee, 1993], and it can differ between chosen domains of the model [Zweers et al., 2010]. WAQUA/DCSM uses a Charnock parameter $\beta_C = 0.032$. In the governing shallow water equations (2.1) and (2.2) that are used in WAQUA/DCSM one can recognise τ_{s_x} and τ_{s_y} in the first term on the right hand side as components of the stress.

In this study, we make a difference between slowly varying wind $\overline{\boldsymbol{u_a}}$, which has variations larger than three hours, and shorter variations $\boldsymbol{u'_a}$. The slowly varying wind corresponds to the synoptic scale wind patterns that are taken from the atmospheric models and used as traditional input into the storm surge model. The time scale of three hours corresponds to the time interval of meteorological input from the ECMWF model (whereas it is 1 hour if HiRLAM input would be used). The shorter term variations (time scales shorter than three hours) are not taken into account[1] and can be considered *unresolved motion*. We describe the total wind as

$$\boldsymbol{u_a} = \overline{\boldsymbol{u_a}} + \boldsymbol{u'_a}. \tag{2.8}$$

Traditionally, in storm surge modelling $\boldsymbol{u'_a} = 0$. This will be compared to experiments with $\boldsymbol{u'_a}$ nonzero, in Monte Carlo experiments, described in chapter 3. Other situations with correlated and uncorrelated noise will be assessed, as well as short term wind fluctuations in longitudinal and lateral direction.

To distinguish between longitudinal and lateral short term motion, as will be done in the Monte Carlo experiments, $\boldsymbol{u'_a}$ and $\overline{\boldsymbol{u_a}}$ will be expressed as longitudinal and lateral wind components. The longitudinal and lateral components are transformed to a Cartesian coordinate system, with the x-axis pointing in the zonal direction and the y-axis pointing in the meridional direction,

$$\boldsymbol{u'_a} = \begin{pmatrix} -\sin\phi & \cos\phi \\ -\cos\phi & -\sin\phi \end{pmatrix} \begin{pmatrix} u' \\ v' \end{pmatrix}, \qquad \overline{\boldsymbol{u_a}} = \begin{pmatrix} -\sin\phi & \cos\phi \\ -\cos\phi & -\sin\phi \end{pmatrix} \begin{pmatrix} U \\ 0 \end{pmatrix}. \tag{2.9}$$

In this expression, ϕ is the mean wind direction[2], u' and v' are longitudinal and lateral components of short term wind fluctuations respectively, and U is the mean wind speed (see Figure 2.4).

[1] As we will see later on, the mean effect of short term wind variations is corrected for via tuning of the model. What is not taken into account is *variation* in these short term fluctuations in space and time.

[2] Wind direction is defined as the direction from which the wind originates in azimuth degrees. The reference vector ($\phi = 0$) is directed north and the angle is taken in clockwise direction.

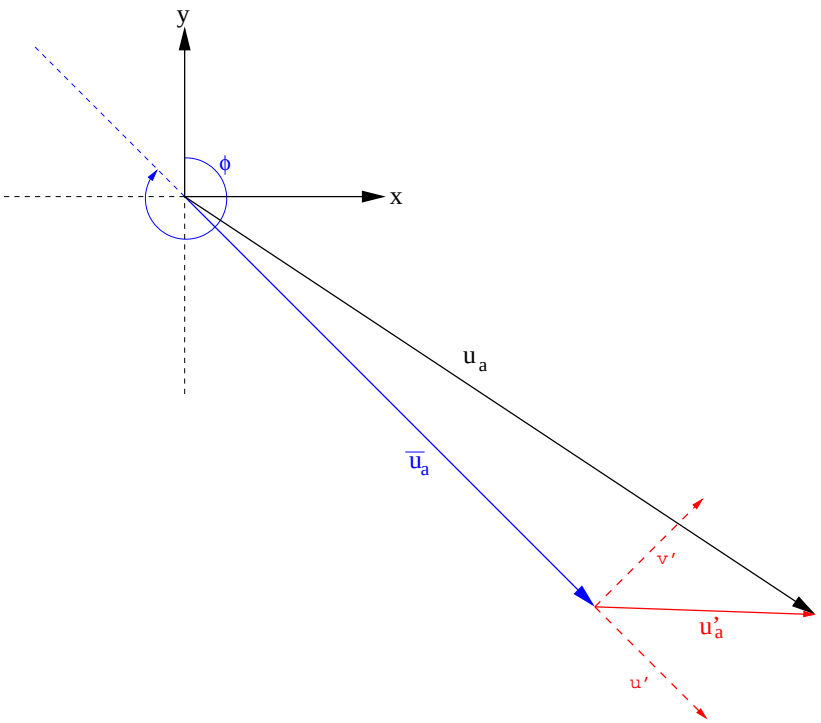

Figure 2.4: Coordinate system with total wind (black) split up in mean wind (blue) and short term deviations (red). In equation (2.9) the wind vector is determined by longitudinal and lateral components and mean wind direction[2].

The averages over the short term fluctuations are

$$\overline{u'} = 0, \quad \overline{u'^2} = \sigma_{u'}^2, \quad \overline{v'} = 0, \quad \overline{v'^2} = \sigma_{v'}^2, \quad \overline{u'v'} = \mathrm{cov}(u', v'), \tag{2.10}$$

where $\sigma_{u'}$ and $\sigma_{v'}$ are standard deviations of short term longitudinal and lateral fluctuations and $\mathrm{cov}(u', v')$ is the covariance between u' and v'.

To calculate the mean stress that is exerted on the sea surface, (2.8) is substituted into (2.6) and averaged in time. A second order Taylor expansion is subsequently performed around $u' = 0$ and $v' = 0$. Assume now that $O(u') \approx O(v') \ll O(U)$ and $O(u')^3$ and $O(v')^3$ are small [Smith and Chandler, 1987]. So higher than second order moments are zero. The resulting mean stress reads

$$\begin{aligned}
\overline{\boldsymbol{\tau_s}} &= \overline{C_d \rho_a \sqrt{(U+u')^2 + v'^2} \begin{pmatrix} -\sin\phi & \cos\phi \\ -\cos\phi & -\sin\phi \end{pmatrix} \begin{pmatrix} U+u' \\ v' \end{pmatrix}} \\
&= C_d \rho_a \begin{pmatrix} -\sin\phi & \cos\phi \\ -\cos\phi & -\sin\phi \end{pmatrix} \begin{pmatrix} \overline{U^2 + u'^2 + 2Uu' + \frac{1}{2}v'^2 + O(v')^3 + O(v')^3 u' + O(v')^3 u'^2 + O(u')^3} \\ \overline{Uv' + u'v' + O(v')^3 + O(v')^3 u' + O(v')^3 u'^2 + O(u')^3} \end{pmatrix} \\
&\simeq C_d \rho_a \begin{pmatrix} -\sin\phi & \cos\phi \\ -\cos\phi & -\sin\phi \end{pmatrix} \begin{pmatrix} \overline{U^2} + \overline{u'^2} + \overline{2Uu'} + \overline{\frac{1}{2}v'^2} \\ \overline{U}\,\overline{v'} + \overline{u'v'} \end{pmatrix} \\
&= C_d \rho_a \begin{pmatrix} -\sin\phi & \cos\phi \\ -\cos\phi & -\sin\phi \end{pmatrix} \begin{pmatrix} U^2 + \sigma_{u'}^2 + \frac{1}{2}\sigma_{v'}^2 \\ \mathrm{cov}(u', v') \end{pmatrix}.
\end{aligned} \tag{2.11}$$

Here, the non-linear impact of wind fluctuations on the mean stress is shown. The result of the mean stress with no fluctuations ($u' = 0$ and $v' = 0$) is increased with terms that contain standard deviation of the short term fluctuations. Note that also the drag coefficient depends on the wind speed. It increases for higher winds and thus increases non-linear behaviour even more.

In order to predict the value of the increased wind stress, we need to derive or specify expressions for the unknowns in the equation (2.11): the second order moments $\sigma_{u'}$, $\sigma_{v'}$ and $\mathrm{cov}(u', v')$. We assume that

the correlation between the short term wind components is small, $\mathrm{cov}(u', v') \approx 0$. Furthermore, the standard deviations of the short term fluctuations can be linked to each other:

$$\sigma_{v'} = r\sigma_{u'}. \tag{2.12}$$

The ratio r is a constant, as follows from considering density spectra of the variation velocity components [Kaimal et al., 1972]. For the longitudinal short term velocity component holds

$$\sigma_{u'}^2 = \overline{u'^2} = \int_0^\infty S_u(n)\, dn, \tag{2.13}$$

where $S_u(n)$ is the spectral density of $\overline{u'^2}$, as a function of the frequency n. Following the 1968 AFCRL Kansas experiments, Kaimal et al. [1972] formulated empirical formulae for the spectra of the turbulent wind components in neutral stratification. After integration of the longitudinal and the lateral spectra,

$$\frac{\sigma_{u'}}{\sigma_{v'}} \approx 1.33. \tag{2.14}$$

Now only one unknown is left to predict the extra stress due to short term deviations. This unknown, $\sigma_{u'}$, is predicted by some atmospheric models, such as ECMWF's atmospheric model. In section 2.2.2 it is explained how $\sigma_{u'}$ is obtained. In this study, we will thus take the standard deviation of the longitudinal wind fluctuations as a measure for short term variations in the atmosphere. In this study this is called *gustiness*.

As we saw before, due to the tuning of the Charnock parameter, the effect of short term motion is already accounted for. What is not properly accounted for however, is *variation* in the short term motion, i.e. higher or lower $\sigma_{u'}$. This is what will be investigated in this study. To do this an atmpherical model and a storm surge model are used. They are introduced in the next section.

2.2 Numerical Models

2.2.1 WAQUA/DCSM

The model that is used in this study is called the Dutch Continental Shelf Model (WAQUA/DCSM, 5$^{\text{th}}$ version) [Gerritsen et al., 1995]. It is a storm surge model that has been developed by the Dutch public works authority (Rijkswaterstaat), Deltares and the Royal Netherlands Meteorological Institute (KNMI). It describes the area of the North Sea, from 48°0′ North to 62°20′ North and from 12° West to 13° East. The spatial resolution is $\frac{1}{8}^{\circ}$ in the zonal direction and $\frac{1}{12}^{\circ}$ in the meridional direction ($\sim$ 8 km), see Figure 2.5. It is based on the WAQUA software package.

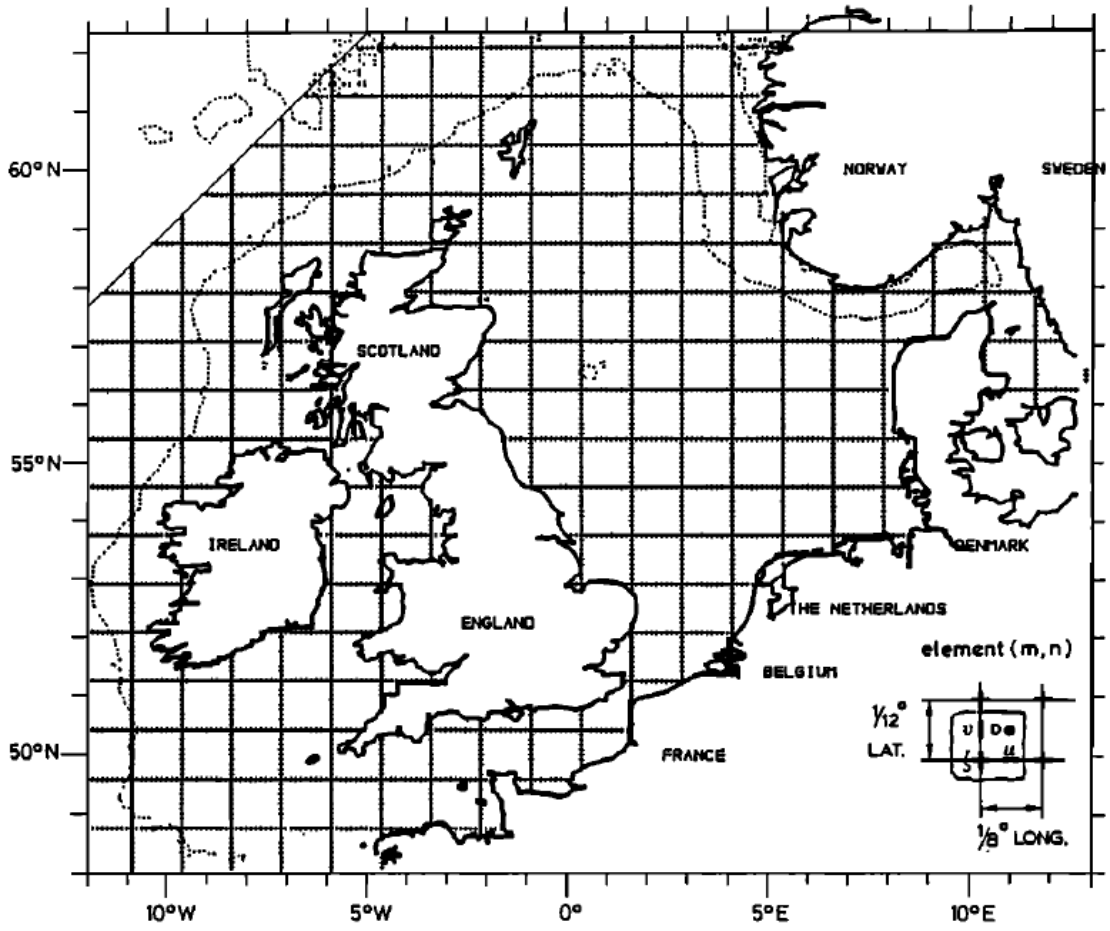

Figure 2.5: 173 × 201 grid of DCSM/WAQUA. After [Gerritsen et al., 1995].

WAQUA/DCSM numerically solves 2-D shallow water equations (2.1), (2.2) and (2.3), transformed into a spherical coordinate system. The model computes the depth averaged currents and sea surface height on every grid point. To increase numerical accuracy, WAQUA/DCSM uses a staggered Arakawa-C grid. It has two open sea boundaries, where a sea level is imposed that corresponds to a sea level due to the 10 tidal constituents O_1, K_1, N_2, M_2, S_2 K_2, Q_1, P_1, NU_2 and L_2 [Gerritsen et al., 1995]. At these boundaries inflow and outflow is allowed. The time step of the model is 10 minutes. It is also possible to run WAQUA/DCSM with a smaller time resolution. In this study, this is done once as a control run. The bathymetry of the concerned area is taken from nautical maps (Figure 2.6).

In operational mode, WAQUA/DCSM runs at the Royal Netherlands Meteorological Institute (KNMI), to make forecasts of sea level hights in the North Sea and provide information to the storm surge warning

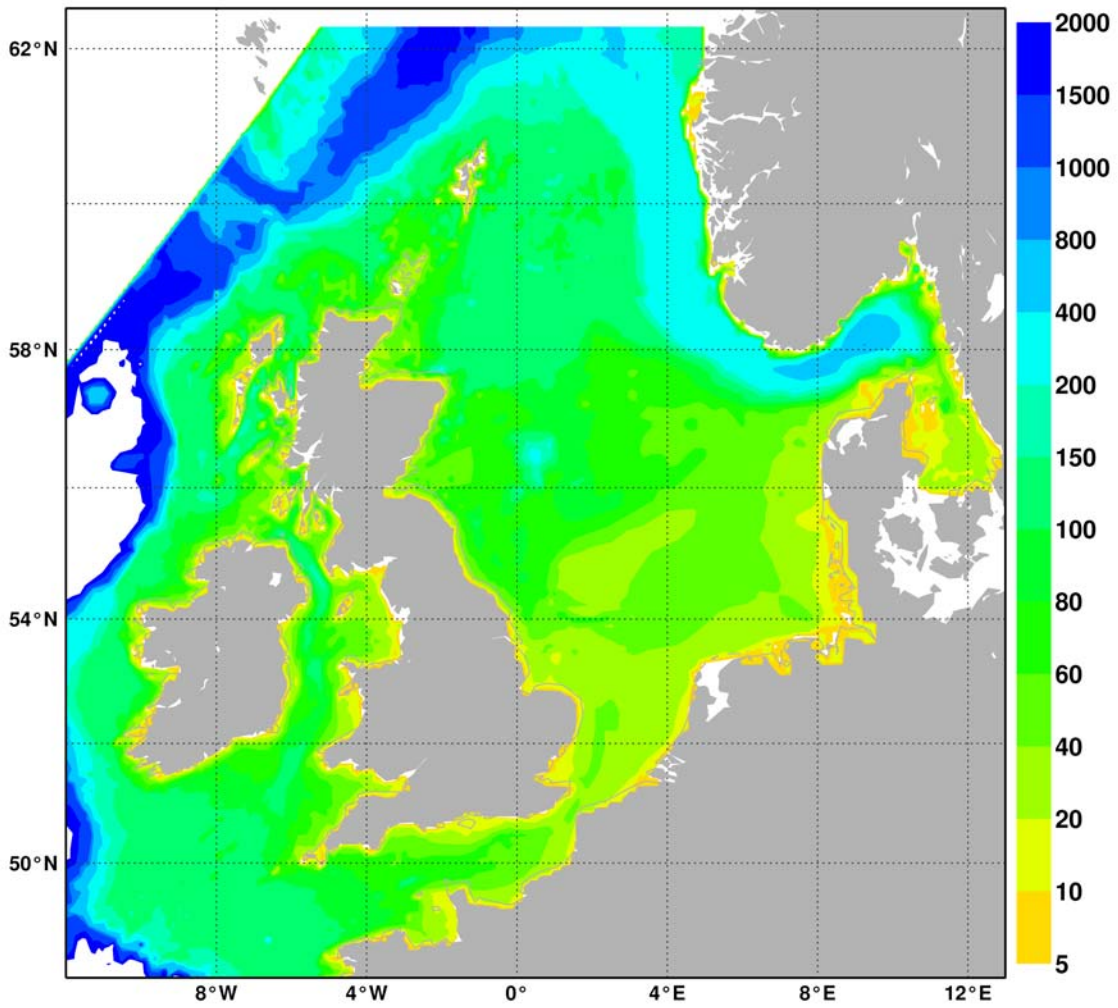

Figure 2.6: Bathymetry of DCSM/WAQUA.

service (SVSD) in the Netherlands. Time series of forecasts are produced for stations along the Dutch and British coast. Some stations that will be used in this study are presented in Figure 2.7.

The meteorological input for the operational WAQUA/DCSM model is obtained from the High-Resolution Limited Area Model (HiRLAM), that gives wind velocity and pressure for every hour at a spatial resolution of 11 km. These wind an pressure fields are linearly interpolated for each time step of the WAQUA/DCSM model. It is also possible to use wind data from the ECMWF atmospherical model, which generates output fields with intervals of 3 hours and a spatial resolution of 16 km. Archived operational forecast fields of the ECMWF model are used in this study. For the air-sea energy exchange the Charnock relation (2.6) is used [Verlaan et al., 2005]. The Charnock parameter β_C has a standard value 0.032 in WAQUA/DCSM. Furthermore, there is the possibility to add a Kalman filter in the model, which assimilates observations of water levels from gauges at the British and Dutch coasts for more accurate results. Since we are interested in the performance of the model, in this study we do not incorporate any data assimilation in WAQUA/DCSM.

2.2.2 ECMWF Atmospheric Model

The ECMWF's Integrated Forecast System is an operational global atmospheric model, which provided the necessary atmospheric data that is used to drive WAQUA/DCSM. It produces a deterministic forecast of 10 days (next to ensemble forecasts) and runs twice a day. It has a spatial resolution of 16 km and 60 vertical

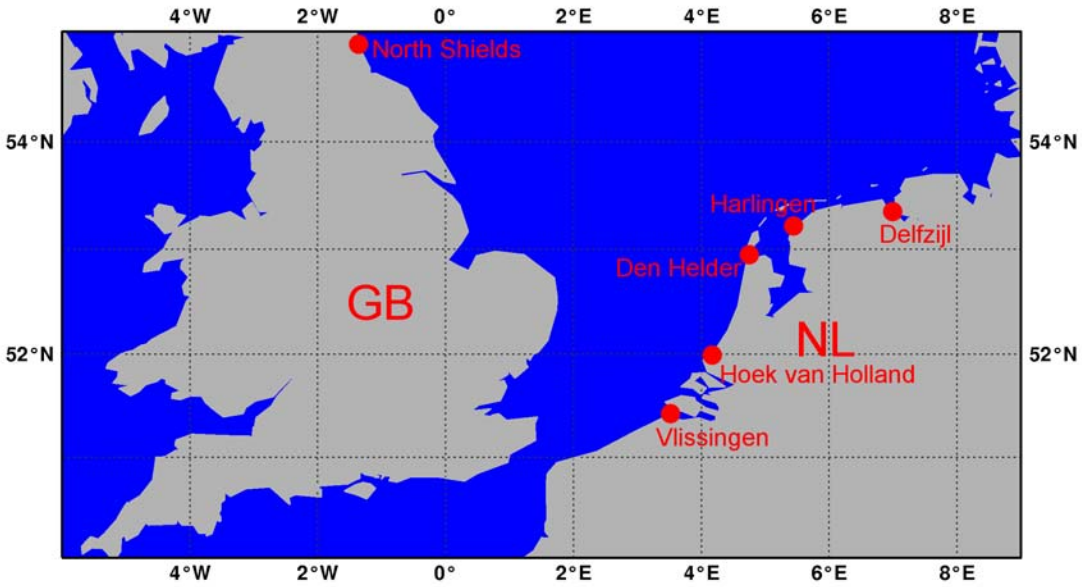

Figure 2.7: Gauges along the Dutch and British coast that are used in this study, for which WAQUA/DCSM generates standard time series. Observations of sea level are also done at these locations.

levels. In this study we only use the output of the ECMWF model.

For storm surge forecasting, the parameters that are normally used are surface wind velocity and sea level pressure. In this study we are also interested in the short term variations of the wind. A parameter that we will use is the standard deviation of the longitudinal short term fluctuations, which we defined as gustiness. We will derive this parameter from the *wind gust* (not to be confused with gustiness). Wind gust is an output parameter of the ECMWF atmospheric model. The wind gust and gustiness are related as follows

$$G = U + g\,\sigma_{u'}, \tag{2.15}$$

where G is wind gust, U is the wind speed, $\sigma_{u'}$ standard deviation of longitudinal short term fluctuations (gustiness) and g is a constant. In the ECMWF model g is taken 2.93. More detailed comments on this as well as more details on wind gust in general are given in appendix A.

Chapter 3

Monte Carlo Experiments

In section 2.1.2 it has been shown that increasing gustiness enhances stress that is exerted on the sea surface. We would like to know what is the impact of this increased stress on the sea level in storm surge situations. To answer this question, different Monte Carlo experiments are performed, that are run with WAQUA/DCSM. Theoretical wind fields are designed, describing a severe storm over the North Sea. In section 3.1.1 a mean wind field and short term deviations in the form of random Gaussian noise are described. In section 3.2.1 distinguished situations are created, with noise in only lateral or longitudinal direction. Furthermore, section 3.4.1 describes more realistic representations of gustiness, with more spatially and temporally correlated noise. Finally, a parameterisation of the added stress as a consequence of short term fluctuations is verified in section 3.6.

3.1 Short term fluctuations as random noise

3.1.1 Method

An idealised storm case and addition of noise for short term fluctuations

To create wind with short term fluctuations, we have designed wind fields following equations (2.8) and (2.9),

$$\boldsymbol{u_a}(\boldsymbol{x},t) = \begin{pmatrix} -\sin\phi & \cos\phi \\ -\cos\phi & -\sin\phi \end{pmatrix} \begin{pmatrix} U(\boldsymbol{x},t) + u'(\boldsymbol{x},t) \\ v'(\boldsymbol{x},t) \end{pmatrix}. \tag{3.1}$$

In this expression, $\boldsymbol{u_a}$ is the wind forcing in grid point $\boldsymbol{x}$ and at time t, transformed to the WAQUA/DCSM coordinate system, ϕ is the wind direction of the mean wind, U is the slowly varying mean wind speed and u' and v' are short term fluctuating longitudinal and lateral wind components, respectively.

In a realistic representation of a wind field, U depends on space $\boldsymbol{x}$ and time t. In chapter 4, we will study some of these situations. Here, the influence of gustiness on a more controlled idealised case is studied. For this purpose we take a mean wind forcing that resembles the forcing that is used by Gill, in his book where he gives an analytical solution of the February 1953 storm in the North Sea [Gill, 1982, pp. 394–403]. A uniform north-westerly wind field is created, parallel to the orientation of the North Sea, i.e. a wind direction of $\phi = 315°$. This is the most effective direction for high storm surges in the Netherlands, because of a long wind fetch. The mean wind speed U of this wind field varies in time, according to a harmonic sine function with a period of 6 days. After 3 days the wind speed is set to zero:

$$U(\boldsymbol{x},t) = \begin{cases} M\sin(\frac{t\pi}{t_s}) & \text{when } 0 \le t \le t_s \\ 0 & \text{when } t > t_s\ , \end{cases} \tag{3.2}$$

with t time, M maximum mean wind speed 25 m/s and t_s is duration of the storm: $t_s = 3$ days. The initial state of the sea level is chosen to be the astronomical tide on 1 January 2009 0 UTC. This state is achieved by running the model over the period of a month without meteorological effects.

Next, we will define how gustiness is introduced into the experiments. We assume that the longitudinal and lateral velocity components of short term fluctuations are Gaussian distributed (as in a neutral boundary layer [Chu et al., 1996]). This corresponds to the assumption that higher than second order moments are zero in equation (2.11). We define $u'(\boldsymbol{x}, t)$ on grid points $\boldsymbol{x} = (x_i, y_j)$, as components of a N-dimensional state vector $\boldsymbol{u'}((j + Bi), t)$. Here, N is the total number of grid points. x_i and y_j are longitude and latitude of the grid point and i and j are column and row of the grid point, counted from the south-west corner. The columns of u' are placed below each other in the state vector, with B the number of grid points along the meridional direction. Now we model

$$\boldsymbol{u'} = \underline{\underline{\boldsymbol{\nu_u}}} \cdot \boldsymbol{D_u}, \tag{3.3}$$

where $\underline{\underline{\boldsymbol{\nu_u}}}$ is an $N \times N$ matrix and $\boldsymbol{D_u}$ is an N-dimensional vector. The components of $\boldsymbol{D_u}$ are drawn from a random number generator, and have a Gaussian distribution with mean 0 and standard deviation 1. With $\underline{\underline{\boldsymbol{\nu_u}}}$, the standard deviation of noise can be manipulated and spatial correlation can be introduced. The same procedure is used to model noise in the lateral direction v'.

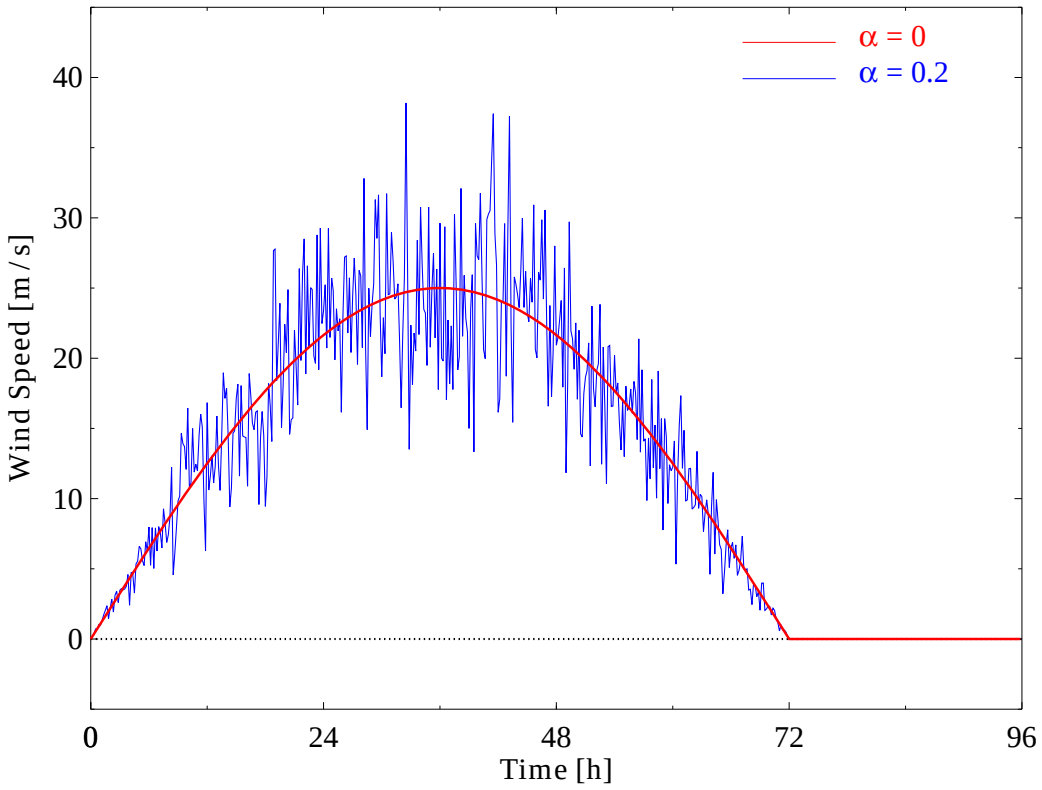

Figure 3.1: Typical wind speed at an arbitrary grid point in a uniform wind field used to show the influence of variations in the wind speed. Wind speed variations relative to the value of the wind speeds are shown with standard deviations of 0 (red) and $0.2\,U$ (blue).

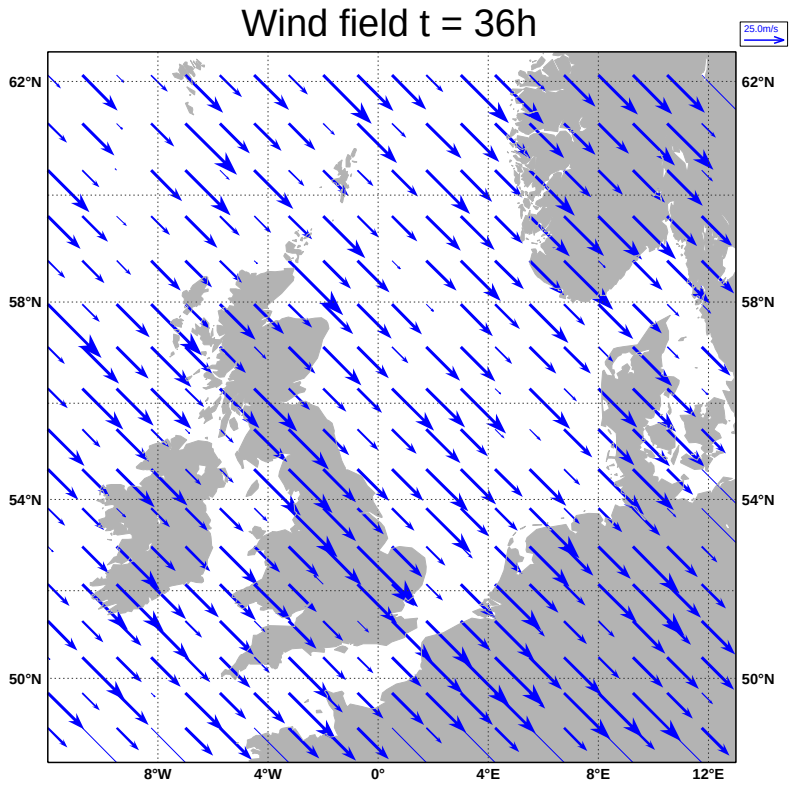

Figure 3.2: Generated wind field at $t = 1.5$ days with added noise: $\sigma_{u'} = 0.2\,U$ and $\sigma_{u'} = 0$. Note: a thinning factor has been used, so not every wind vector of every WAQUA/DCSM grid point is plotted.

Every time step t_k of the model a new noise field is generated. In this case the time step in 10 minutes, so the short term fluctuations have a time scale of 10 m. This time scale is relatively short to compared to the physical processes of a storm surge and Kelvin waves. It is also shorter than the traditional time scales of the meteorological input, which are 1 or 3 hours for HiRLAM or ECMWF, respectively. So the noise represents unresolved motion of the wind.

Short term wind fluctuations as random noise

From (3.3) short term wind fluctuations are generated by the addition of random noise. As a first suggestion we add random noise. To obtain noise with standard deviations $\sigma_{u'}$ and $\sigma_{v'}$:

$$\begin{aligned} \underline{\underline{\boldsymbol{\nu_u}}} &= \sigma_{u'}\underline{\underline{I}} \quad \text{and} \\ \underline{\underline{\boldsymbol{\nu_v}}} &= \sigma_{v'}\underline{\underline{I}}, \end{aligned} \tag{3.4}$$

where $\underline{\underline{I}}$ is the identity matrix. We chose gustiness proportional to the mean wind speed, i.e. $\sigma_{u'} = \alpha_u\,U(t)$ and $\sigma_{v'} = \alpha_v\,U(t)$. In (2.14) it is shown that the ratio of the standard deviation in the longitudinal and lateral direction is approximately 1.33 for neutral conditions. This number is used to perform an initial experiment, with $\alpha_u = 0.4$ and $\alpha_v = 0.3$. Values of 0.3 and 0.4 times the mean wind speed, are relatively high values for the standard deviation of short term fluctuations.

In operational mode WAQUA/DCSM uses only slowly varying mean wind. That means that $u'(\boldsymbol{x}, t) = 0$. We compare this case without noise to the case with added random noise. In Figure 3.1 a typical time series

of wind speed is shown, which is generated for an arbitrary grid point, for a case with and without added random noise. The harmonic function can clearly be recognised, as well as the added random noise.

A typical wind field with longitudinal random noise is shown in Figure 3.2. The arrows denote the wind vectors. In this figure there are only variations in the longitudinal wind. The addition due to short term variations u' is independent of space. This case will be treated further in Experiment 2 in 3.2.1.

To examine the sensitivity of the sea level at a certain location to the amount of noise, an ensemble of 50 realisations with random noise is made. This means that a new set of random numbers is drawn for $\boldsymbol{D_u}$ and $\boldsymbol{D_v}$, in (3.3). Of course, the statistical characteristics of $\boldsymbol{u'}$ and $\boldsymbol{v'}$ remain the same, but the generated wind fields are not identical. The experiment is repeated for various angles of the mean wind, ϕ in (3.1). In this way, the influence of the orientation of the mean wind with respect to the basin (North Sea), is determined.

3.1.2 Results

Sea level

In section 3.1.1 we described how experiments were set up with random noise in longitudinal and lateral direction ($\alpha_u = 0.4$ and $\alpha_v = 0.3$). These are compared to a case without noise. First we will look at plots of the sea level and the surge in the North Sea area. In Figure 3.3, sea surface height of a run without added noise at $t = 12$ hours, is presented. A a tidal wave can be recognised. Beside the tidal wave, a storm surge contributes to the water level. So after subtracting the astronomical tide, only the level due to the storm surge is found. This is shown in Figure 3.4. As expected the surge increases towards the Dutch coast on the southern side of the North Sea. The surge varies along the coast and in the Netherlands a surge is found from 1.2 up to 2.8 meters.

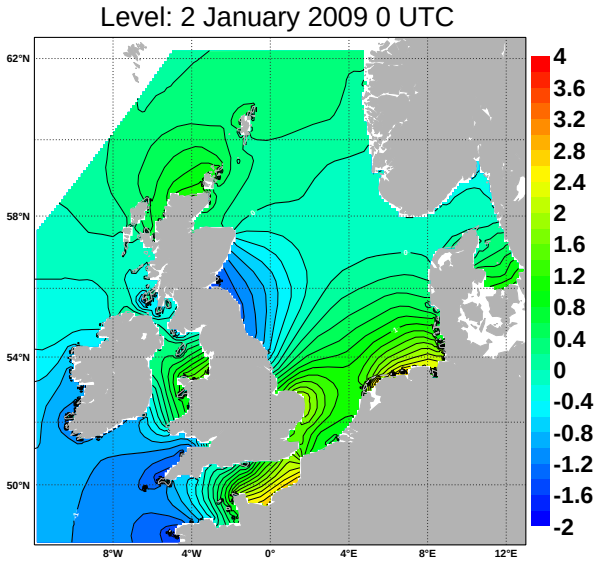

Figure 3.3: Sea level [m] of no noise run.

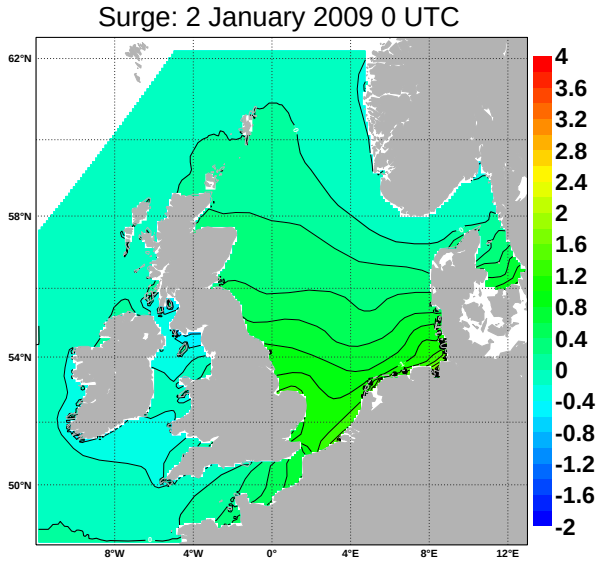

Figure 3.4: Surge [m] of no noise run.

Similar plots for model for the ensemble with added random noise, with $\alpha_u = 0.4$ and $\alpha_v = 0.3$, are shown in Figures 3.5 and 3.6. Again a tidal wave is observed. The contour lines of the water level show the influence of the added random noise, in their more irregular pattern. Remarkable in comparison with Figures 3.3 and 3.4, is the increase of the surge level at $t = 12$ hours. The surge along the Dutch coast varies from 1.6 meters upwards. Contours of equal sea surface height move north, when comparing the random noise run, with the run without noise. This indicates that adding noise to the wind field enhances a storm surge. We have to keep in mind that these Figures 3.5 and 3.6 are the fields of only one realisation of a random noise run. An ensemble of 50 realisations will be presented now to see whether this conclusion can be verified.

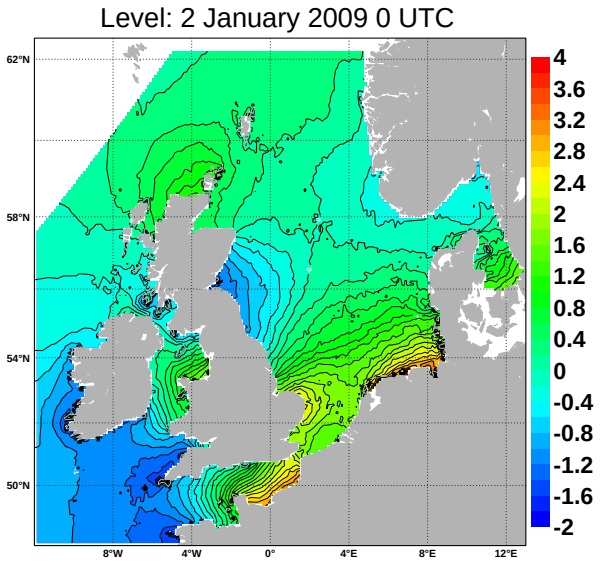

Figure 3.5: Sea level [m] of one realisation of the run with random noise in longitudinal and lateral direction: $\alpha_u = 0.4$ and $\alpha_v = 0.3$.

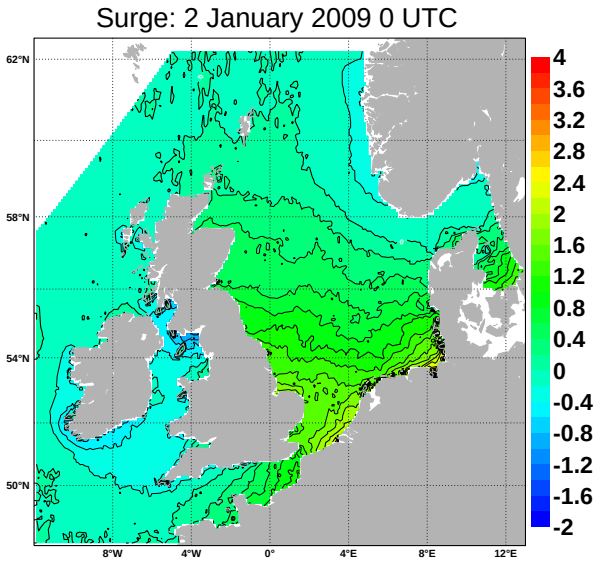

Figure 3.6: Surge [m] of one realisation of the run with random noise in longitudinal and lateral direction: $\alpha_u = 0.4$ and $\alpha_v = 0.3$.

Time series of ensemble

This increase of sea level due to random noise is made clear in plots of a time series at a fixed location at the coast. In Figure 3.7 a time series is shown at Hoek van Holland. This is a station that is representative for the stations along the Dutch coast, and the behaviour of the surge is comparable that in other stations. The figure shows the run without noise in red. The blue dotted line represents the astronomical tide from 1 January 2009 on. Clearly, as soon as the wind speed increases (Figure 3.1) the sea level rises above the level of the astronomical tide. The shape of superimposed tidal variations are recognised. After the wind speed is set zero, the surge ceases and a small negative surge is observed around 4 January 0 UTC, following on the preceding large positive surge.

A run with added random noise in longitudinal and lateral direction, as described in section 3.1.1, is the blue line in Figure 3.7. It is not as a smooth line as the no noise run, but the main features are the same: a surge superimposed on the astronomical tide. It can be recognised that the sea level of the runs with noise lies considerably higher than that of the run without noise.

To examine the sensitivity of the sea level at a certain location to the amount of noise, an ensemble of 50 realisations of the random noise run is performed. The 50 realisations are plotted in orange in Figure 3.7. One can observe that all the 50 realisations lie above the no noise run, when a positive surge is generated. They lie below the no noise run, around 4 January 0 UTC, when there is a small negative surge. In a plot of the surge, in Figure 3.8, these effects are also visible. Also the resemblance with a time series of the wind forcing (Figure 3.1) is found. In a plot of only the surge in Figure 3.8 this effect is even clearer.

We conclude that addition of random noise to the wind field amplifies the surge that is obtained at the Dutch coast. When investigating different mean wind directions and locations in the North Sea, we will expand this conclusion.

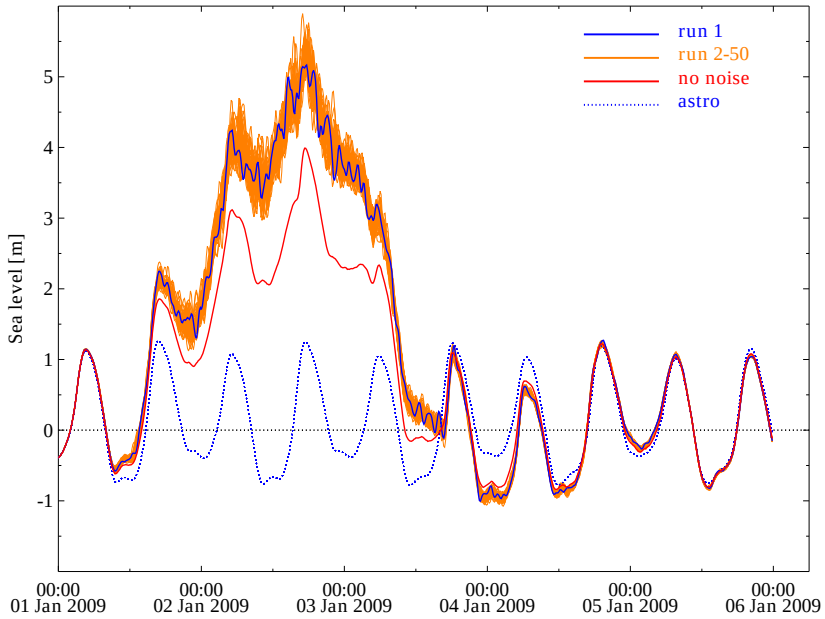

Figure 3.7: Sea level in Hoek van Holland of 50 ensemble runs with random noise in longitudinal and lateral direction: $\alpha_u = 0.4$ and $\alpha_v = 0.3$ (orange lines and blue line). Red line is the no-noise run. The blue dotted line denotes the astronomical tide.

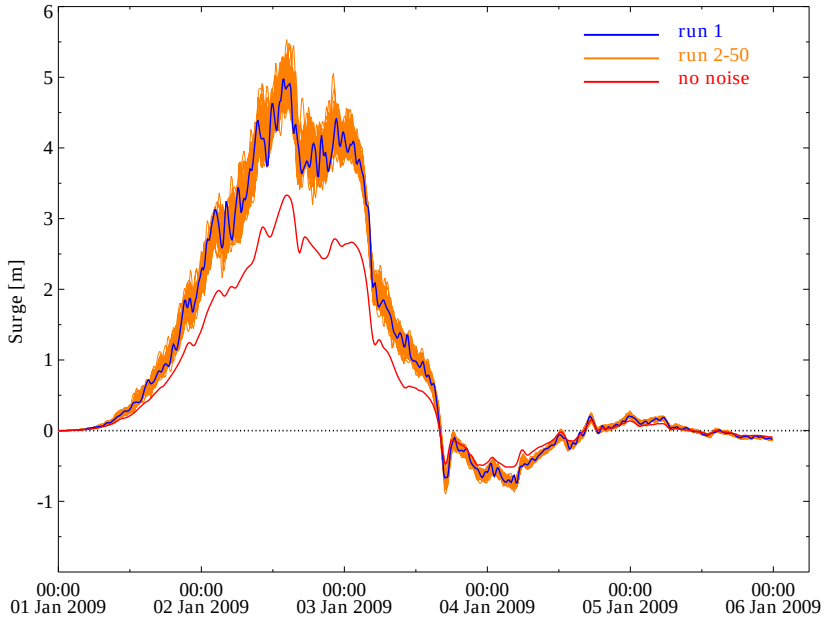

Figure 3.8: Surge in Hoek van Holland of 50 ensemble runs with random noise in longitudinal and lateral direction: $\alpha_u = 0.4$ and $\alpha_v = 0.3$ (orange lines and blue line). Red line is the no-noise run.

Surge characteristics for different wind directions

The effect of the addition of noise on the surge is studied further in Figure 3.9. In this case we vary the angle of the mean wind. This is done in the following way. In section 3.1.1 we described how wind fields with added random noise have been created. We exactly follow the same procedure for 50 ensemble runs, but now we change ϕ in equation (3.1). So now we take, e.g. $\phi = 0°$ or $\phi = 180°$. Angle ϕ is increased twelve times, in steps of 30°, thus: $\phi = 0°, \phi = 30°, ..., \phi = 300°, \phi = 330°$. Finally 12 ensemble runs of each 50 realisations are obtained. This is done for gauge Hoek van Holland and gauge North Shields, which lies on the other side of the North Sea basin in Great Britain (see Figure 2.7 for the locations of the gauges).

In Figure 3.9 the surge is shown as a function of the angle of the mean wind (red line). This is the surge of the random noise runs at 2 January 14 UTC, two hours after the wind speed has reached its maximum. The surge presented here is the mean of the 50 realisations. The blue line indicates the variation of the surge at a certain angle, in the form of the standard deviation of the 50 realisations.

As expected, the surge in Hoek van Holland is highest with wind from the north and west; angles 270° to 360°. In these cases the mean wind is directed towards the Dutch coast. When the angle is changed from there, the surge decreases up to a negative surge of about 4.5 meter for a south easterly wind, away from the coast. Surprisingly, the surge that is found at the English coast has a consistent behaviour with the one at Hoek van Holland. An easterly wind is directed towards the coast in North Shields and a positive surge is expected, but still a negative surge is found. An explanation for this might be that the angle of the wind with respect to the orientation of the whole North Sea is more important than the angle of the wind with respect to the coast. So one should think of mechanisms that the water is pushed into the basin or dragged out of the basin by the wind stress. This effect is than more important than local effects, such as the wind angle with respect to the coast. Notice here that we use an extremely extended and strong wind field (mean wind is uniform in space). Local effects will be important when more detailed varying wind fields are used.

Next, results of runs with noise in the wind speed are compared to the results of the run without any noise. The difference of the average of the sea level of the ensemble runs with noise and the run without noise is presented with the black line in Figure 3.9. It should be notified that the addition due to white noise is in phase with the surge. This means that the addition of noise decreases a negative surge and increases a positive surge. This addition due to noise is significant since it is larger than the standard deviation of the sea level of the 50 runs.

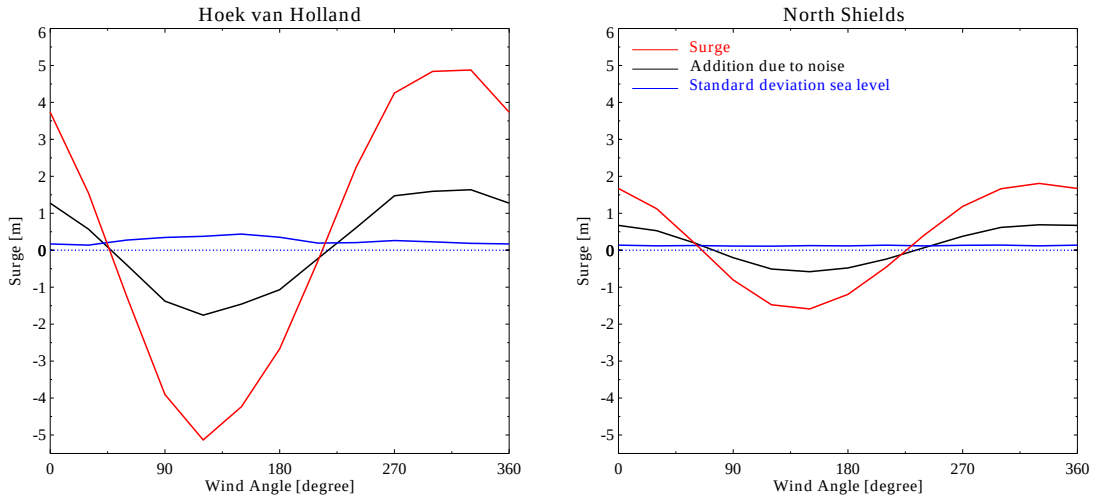

Figure 3.9: Surge averaged over 50 ensemble runs as a function of the angle of the wind represented by the red line. In black the difference of the mean of the sea level of 50 ensemble runs with random noise and the run without random noise. The blue line represents the standard deviation of the sea level of the 50 ensemble runs with random noise.

3.2 Longitudinal and lateral short term wind fluctuations

3.2.1 Method

It is interesting to investigate the influence of longitudinal and lateral noise separately. We would like to know which component elevates the surge most. We expect that the longitudinal noise contributes most. What is the role of lateral noise is less clear. Does it increase or decrease a surge? From equation 2.11 in the theory section, we would expect a small positive contribution of the lateral noise as well. Some simple experiments are performed in addition to the one described above:

1. In the first experiment the longitudinal noise level is kept the same as in section 3.1, but lateral noise is neglected: $\alpha_u = 0.4$, $\alpha_v = 0$. Now the influence of only variations in de direction of the slowly varying wind can be shown.

2. Longitudinal noise with lower intensity: $\alpha_u = 0.2$, $\alpha_v = 0$. Noise which is a factor 0.2 times the mean wind speed is a realistic value that can be found over water.

3. To study the effect of lateral noise, longitudinal noise is neglected in the same way: $\alpha_u = 0$, $\alpha_v = 0.4$. Note: the lateral component of the noise is increased here, compared to the experiments before, where lateral noise level of $\alpha_v = 0.3$ is used.

Again an ensemble of 50 realisations is created, to find out about mutual variation. Also the no-noise run has been used as comparison to the ensemble run.

3.2.2 Results

We compare results of ensemble runs with $\alpha_u = 0.4$ and $\alpha_v = 0$ (experiment 1) to the results of the ensemble: $\alpha_u = 0.4$ and $\alpha_v = 0.3$, that is described in section 3.1.1. This is shown in Figure 3.10. The green lines represent the ensemble of 50 realisations with only longitudinal noise. The orange lines are the realisations with both longitudinal and lateral noise is shown. The red curve denotes the no noise run: $\alpha_u = 0$ and $\alpha_v = 0$. The blue line and the pink line show the average of all orange and green realisations, respectively.

One can observe that the surge is amplified due to added noise, although it is a little less strong than with noise in both longitudinal and lateral direction. Apart from that, the overall behaviour is similar. Figure 3.11 shows that noise in the lateral direction also contributes in a small amount to the amplification. The realisations with $\alpha_u = 0$ and $\alpha_v = 0.4$ (experiment 3), here denoted in green and pink, enhance the surge with respect to the red line of the no-noise run. However, this effect is weaker than that of only noise in longitudinal direction (even more when taken into account that the level of lateral noise has increased).

When the amount of noise is decreased, as is done in the case with $\alpha_u = 0.2$ and $\alpha_v = 0$ (experiment 2), depicted in Figure 3.12 by the green and pink lines, also the amplification gets weaker.

3.3 Longitudinal short term wind fluctuations with higher cut-off frequencies

In this experiment the time step of WAQUA/DCSM is reduced. In this way more noise fields are created in the same time range, so the cut-off frequency of the short term fluctuations is increased. This is done to check the importance of higher frequency noise. A time step of 1 minute was used, instead of 10 minutes and $\alpha_u = 0.4$, $\alpha_v = 0$. The level of noise (standard deviation of random noise) is the same as in experiment 1 in section 3.2.1.

The result is shown in Figure 3.13. The 50 realisations with a time step of 10 minutes are denoted by the green curves. The pink line is a (single) run with time step 1 minute. The run with time step 1 minute does not deviate distinctively from the ensemble with time step 10 minutes. We conclude that the addition of higher frequencies in the noise is not important at this stage, and we decided not to investigate the effect of changing the time step and higher frequent fluctuations any further.

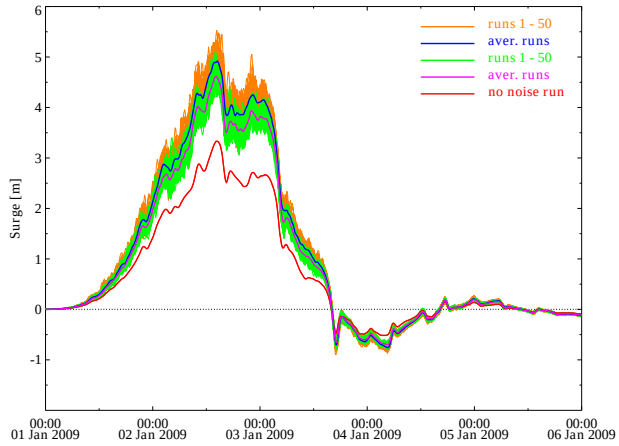

Figure 3.10: Surge in Hoek van Holland of 50 ensemble runs with random noise in longitudinal and lateral direction: $\alpha_u = 0.4$ and $\alpha_v = 0.3$ (orange lines). Idem with random noise runs only in longitudinal direction: $\alpha_u = 0.4$ and $\alpha_v = 0$ (green lines). The blue and pink curves denote the average of the orange and green results, respectively. The red line denotes the surge of the no-noise run.

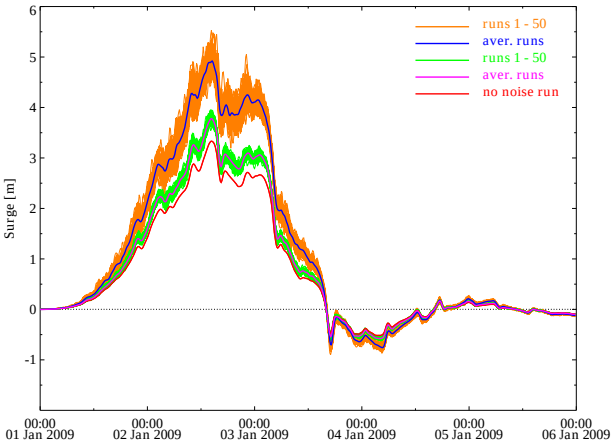

Figure 3.11: Surge in Hoek van Holland of 50 ensemble runs with random noise in longitudinal and lateral direction: $\alpha_u = 0.4$ and $\alpha_v = 0.3$ (orange lines). Idem with random noise runs only in lateral direction: $\alpha_u = 0$ and $\alpha_v = 0.4$(green lines). The blue and pink curves denote the average of the orange and green results, respectively. The red line denotes the surge of the no-noise run.

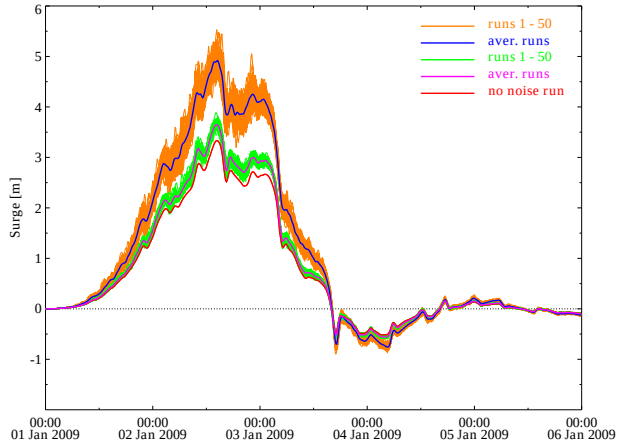

Figure 3.12: Surge in Hoek van Holland of 50 ensemble runs with random noise in longitudinal and lateral direction: $\alpha_u = 0.4$ and $\alpha_v = 0.3$ (orange lines). Idem with low random noise runs only in longitudinal direction: $\alpha_u = 0.2$ and $\alpha_v = 0$ (green lines). The blue and pink curves denote the average of the orange and green results, respectively. The red line denotes the surge of the no-noise run.

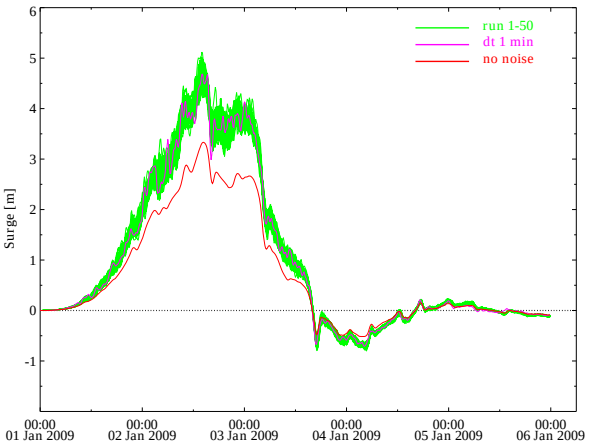

Figure 3.13: Surge in Hoek van Holland of 50 ensemble runs with random noise only in longitudinal direction: $\alpha_u = 0.4$ and $\alpha_v = 0$, with a time step of 10 minutes (green lines). Idem with random noise runs only in longitudinal direction: $\alpha_u = 0.4$ and $\alpha_v = 0$, with a smaller time step of 1 minute (pink line). The red line denotes the surge of the no-noise run.

3.4 Gustiness as spatially correlated noise

3.4.1 Method

In section 3.1.1 a wind field was created with noise that is independent of time and space. This means that wind at one grid point is not influenced by a neighbouring grid point or by data points of any time steps back. One could imagine that in the atmosphere correlation in time and space is existent. One should think for instance of development of convective cells and showers. In these experiments we investigate whether added correlation is space and time influences the resulting surge in the North Sea.

This is why two additional experiments are designed, with $\sigma_{u'} = 0.4\,U$ and $\sigma_{v'} = 0$ as standard deviations of the short term wind components. These values correspond to experiment 1 of section 3.2. The slowly varying wind field is the same as in equation (3.2). Also, $\phi = 315°$, thus a uniform northwesterly wind is created. In the first experiment, spatial correlation is added in the noise function, that determines u'. In the second experiment in section 3.5.1, correlation in both space and time will be added through the noise function. The average standard deviations of the wind field for every time step is still the same as in the experiments of section 3.1.1, but wind on neighbouring data points and time steps is disturbed with higher mutual correlation.

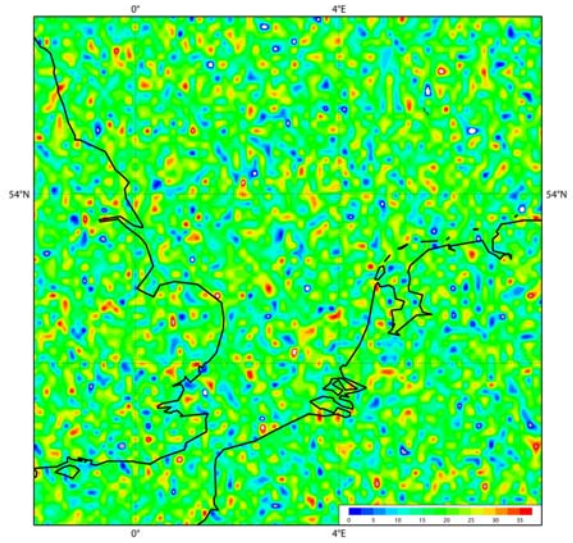

Figure 3.14: Zonal component of the wind for added random noise. $t = 24h$

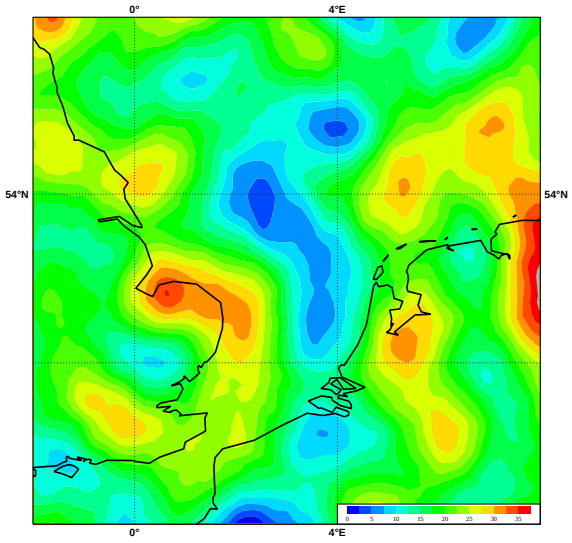

Figure 3.15: Zonal component of the wind for added correlated noise. $t = 24h$

Creation of spatially correlated wind fields

To introduce spatial correlation into the field, we generate random noise fields again. But now, instead of taking only random noise, as was done in the preceding sections, we average locally over the noise values in the neighbouring grid points. The averaging is not done uniform is space, values in grid points that are near are given more weight than those that are far away.

This urges for a clear definition of the location of grid points and their neighbours. As is used in chapter 3.1.1 the location of a grid point is given by: $\boldsymbol{x} = (x_i, y_j)$, where x_i and y_j are longitude and latitude of the grid point and i and j are column and row of the grid point, counted from the south-west corner. The location of a neighbour is defined as $\hat{\boldsymbol{x}}(x_{\hat{i}}, y_{\hat{j}})$, with $x_{\hat{i}}$ and $y_{\hat{j}}$ longitude and latitude of the neighbour and $\hat{i}$ and $\hat{j}$ are column and row of the neighbour.

While we average over the neighbours, we use a weighting factor w that decreases for increasing distance from the grid point. In other words, the matrix $\underline{\underline{\boldsymbol{\nu_u}}}$ in equation (3.3) is not taken the unit matrix anymore. A simple example of how this averaging is carried out and how this is represented by $\underline{\underline{\boldsymbol{\nu_u}}}$ is given in appendix B.

In this experiment, the neighbours within a radius of 10 grid points contribute to the noise in a grid point. The weight of the neighbour contribution decreases linearly to zero with the distance.

$$w(\hat{j} + B\hat{i},\, j + Bi) = \max(1 - 0.1\sqrt{(\hat{i} - i)^2 + (\hat{j} - j)^2}, 0), \tag{3.5}$$

where w are the weights of the neighbours as elements in $\underline{\underline{\boldsymbol{\nu_u}}}$.

So instead of $\underline{\underline{\boldsymbol{\nu_u}}} = \sigma_{u'}\underline{\underline{I}}$, we have:

$$\underline{\underline{\boldsymbol{\nu_u}}} = \gamma \begin{pmatrix} w(1,1) & w(2,1) & \dots & w(N,1) \\ w(1,2) & w(2,2) & & \vdots \\ \vdots & & \ddots & \vdots \\ w(1,N) & \dots & \dots & w(N,N) \end{pmatrix}. \tag{3.6}$$

$\boldsymbol{u'}$ becomes

$$\boldsymbol{u'} = \gamma \begin{pmatrix} w(1,1) & w(2,1) & \dots & w(N,1) \\ w(1,2) & w(2,2) & & \vdots \\ \vdots & & \ddots & \vdots \\ w(1,N) & \dots & \dots & w(N,N) \end{pmatrix} \cdot \boldsymbol{D_u}. \tag{3.7}$$

A constant γ is used to maintain the same variance in the random wind field as in the experiments before, i.e. $\sigma_{u'} = 0.4U$. This resulted in $\gamma = 5.8$. In the experiment done here, only longitudinal short term fluctuations are considered, so v' is taken zero again.

Figures 3.14 and 3.15 show the effect of the operation that is explained above. The zonal component of the wind at $t = 24h$ is shown for the cases with random noise and spatially correlated noise. Values range from 0 m/s (blue) to 35 m/s (red). In the field with added correlation, we see clear structures and patterns in the wind field. Similarities showers of squall lines are visible. Note: in this experiment, every time step the procedure is repeated, so a new unique noise field is created. The patterns that are shown here are thus not consistent in time and therefore not yet realistic. Correlation in time will be added later on in section 3.5.1. One can also question whether the scale of the correlation is chosen correctly. Correlation can also happen on other scales. However, here we would like to show qualitatively what would happen to the result if we add some sort of correlation. In this rather idealised experiment this level of realism satisfies.

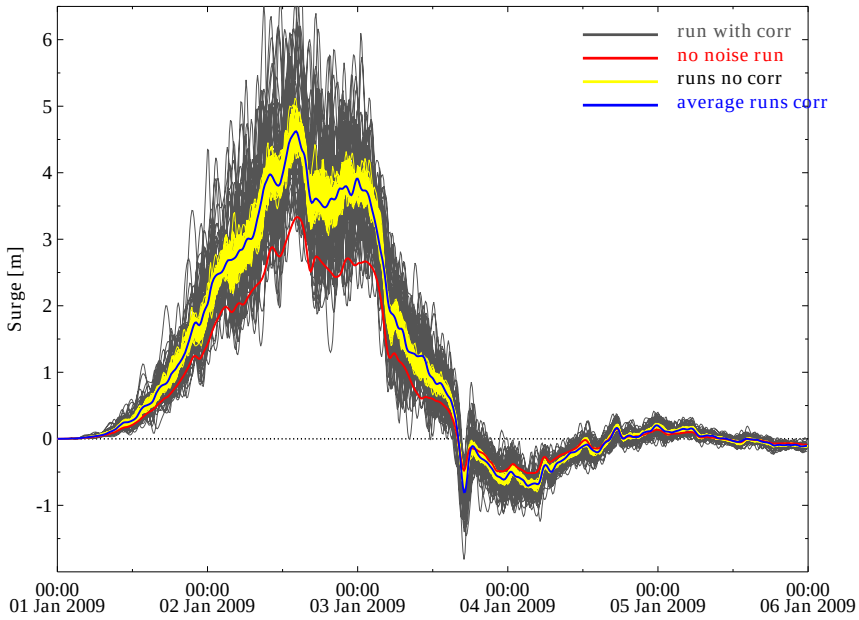

Figure 3.16: Surge in Hoek van Holland of 50 ensemble runs with spatially correlated noise runs only in longitudinal direction (black lines). The blue line is the average of these runs. Surge in Hoek van Holland of 50 ensemble runs with uncorrelated noise runs only in longitudinal direction (yellow lines). Red line is the no noise run.

3.4.2 Results

Figure 3.16 shows a time series of the surge at Hoek van Holland of 50 ensemble runs with spatially correlated noise. The black lines represent the runs with correlated noise. The yellow lines represent the corresponding no-correlation runs. These are the same as the green lines in Figure 3.10. The red line is again a no-noise run. The blue line shows the mean of the 50 ensemble runs with correlation.

The addition of correlation in the noise vector does not influence the average surge. The line, representing this average, lies within the narrow area of the no-correlation noise runs. So, on average, the correlated noise enhances the surge in the same amount as for runs without correlated noise. The variation between the runs with added spatial correlation however, has increased considerably. The band of different runs is much wider than that of runs with uncorrelated noise.

We can explain this by looking at the noise field. When we have a noise field with spatial patterns, probability is high that two neighbouring grid points have similar fluctuations. The local impact of the fluctuations will be higher, when neighbouring points are 'acting together'. This explains why the mutual variation between different realisations is higher than in the experiments without correlation.

3.5 Gustiness as both spatially and temporally correlated noise

3.5.1 Method

After that we investigated only correlation in space, we would like to know the impact of wind fields with correlation in space and time on a surge. We imagine a wind field with high spatial and temporal correlation as wind field, like we have in Figure 3.15, passing by in a stationary flow in the atmosphere. It is a simple and idealised representation of an atmospheric flow. Again one can question it's correspondence with reality, but it is used to get a general idea what would be the qualitative impact of the addition of correlation in time and space.

We chose to shift the noise field one grid point to the east and two to the south per time step, which corresponds to a northwesterly flow of about 30 m/s. Every time step spatially correlated noise from equation (3.7) is added to the noise function that was shifted:

$$\boldsymbol{u'}(x_i, y_j, t_k) = \epsilon\, \boldsymbol{u'}(x_{i-1}, y_{j-2}, t_{k-1}) + (1-\epsilon)\, \underline{\underline{\boldsymbol{\nu_u}}} \cdot \boldsymbol{D_u}(t_k). \tag{3.8}$$

The first term in this equation gives the shifted field, the second term gives a distortion of spatially correlated noise on that field . This distortion is generated in the same way as in the experiment with only spatially correlated noise, that is described above. Parameter ϵ is taken 0.75 here. Again only noise in the longitudinal direction is taken into account. γ in equation (3.6) is taken 15.0. This is higher than before, because there has been more averaging of noise values.

In Figure 3.17 an example is shown of the correlation in time and space of a wind field. The graph on the left shows the autocorrelation of a time series of the wind speed. The correlation is high for short time scales. It decreases to 0.6 for time steps larger than one hour. In the image on the right hand side the effect of spatial correlation is shown. It is the auto correlation of wind speeds of data points along latitude 54° N. Here, one can see that spatial correlation decreases for increasing distances.

The comparison with the same plots of wind fields without added correlation, which are created in section 3.1.1, is presented in Figure 3.18. It is clear that in the case of no added correlation to the noise field the lines decrease rapidly towards 0.5 and zero. An autocorrelation of 0.5 can be attributed to the contribution of the slowly varying wind signal U, that changes on the time scale of days and adds deviations from the mean wind speed (in time). This is not the case with the spatial correlation, which declines to zero, because U is uniform and thus does not deviate from the mean wind speed (in space).

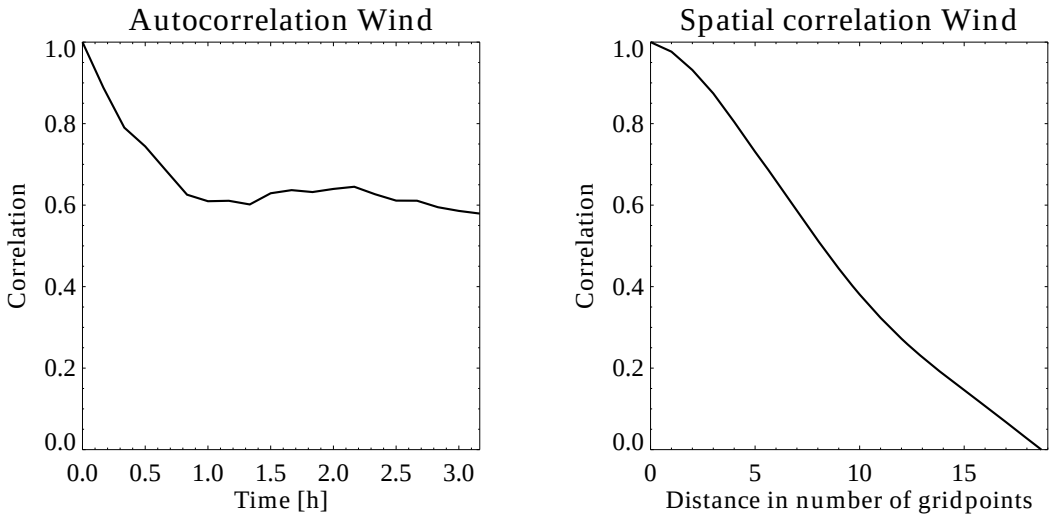

Figure 3.17: Auto correlation of a time series of the wind speed for data point at 54° N and 4° E (left) of the wind fields with added spatial and temporal correlation. Spatial correlation of a data set of the wind speed at t = 36 h along the the latitude 54° N (right).

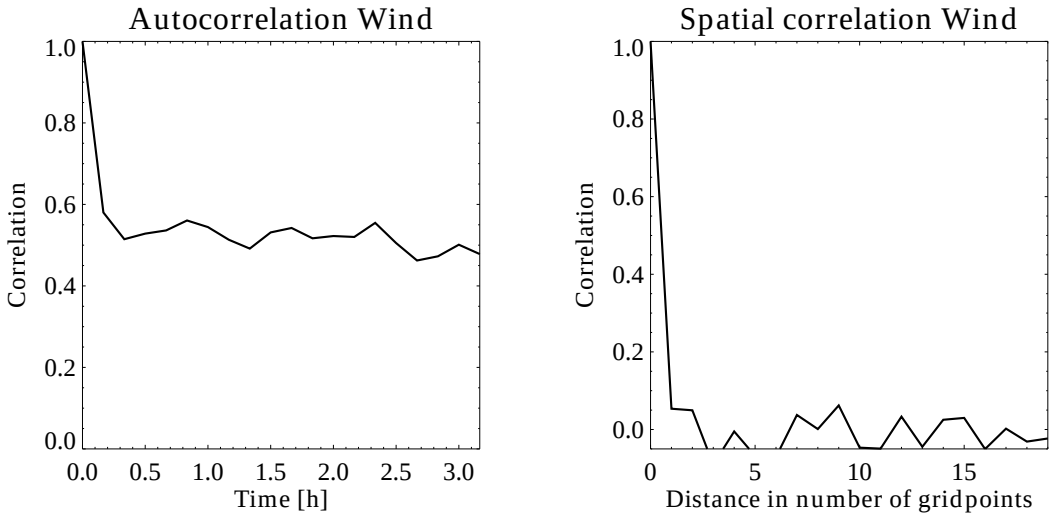

Figure 3.18: Auto correlation of a time series of the wind speed for data point at 54° N and 4° E (left) of the wind fields without added correlation. Spatial correlation of a data set of the wind speed at t = 36 h along the latitude 54° N (right).

3.5.2 Results

In Figure 3.19 the results are presented. Similar as in Figure 3.16, the black lines represent sea levels of 50 realisations with spatial and temporal correlation. The blue line is the average of the 50 realisations. The yellow lines are sea levels of the random noise runs. The red line represents the no-noise run.

Again, we recognise that the average of the 50 realisations with added correlation in time and space is close to the runs without correlation. So, also the addition of temporal correlation does not affect the surge on average. The variation between the ensemble runs is considerably higher than without added correlation.

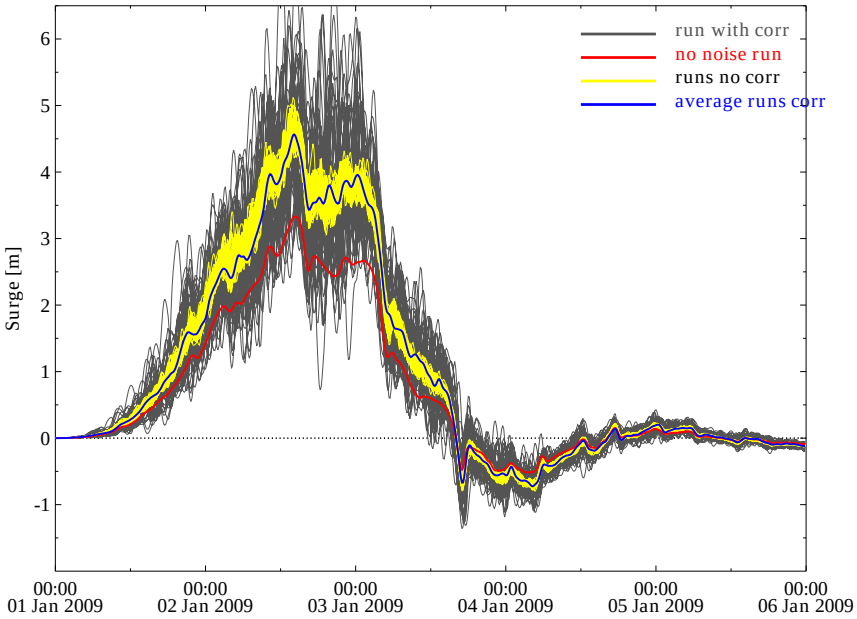

Figure 3.19: Surge in Hoek van Holland of 50 ensemble runs with spatially and temporally correlated noise runs only in longitudinal direction (black lines). The blue line is the average of these runs. Surge in Hoek van Holland of 50 ensemble runs with uncorrelated noise runs only in longitudinal direction (yellow lines). Red line is the no noise run.

Results from 3.4 and 3.5 are summarised in Figure 3.20, where standard deviations of the ensembles with correlated noise are presented. This time series is based on the 50 realisations of the surge at Hoek van Holland. The orange line represents the standard deviation of the realisations with spatially correlated noise. The black line is the standard deviation of the runs with spatially and temporally correlated noise. The standard deviation is high when correlation in space is added, maximum 1.0 meter at 2 January. The shape of the orange and black lines are similar, so standard deviation is not enhanced further due to the addition of correlation in time in the noise. In both cases, the variations between runs are large compared to the average deviation from the uncorrelated runs, represented by the green and red lines (the average of the correlated runs minus the average of the uncorrelated runs).

It is important to acknowledge that this variation between runs increases so much for added correlation. It infers that, in more realistic situations with more spatial and temporal correlation, the maximum level of the surge, which is important for coastal protection, can be higher and varies more in different situations with the same statistical characteristics.

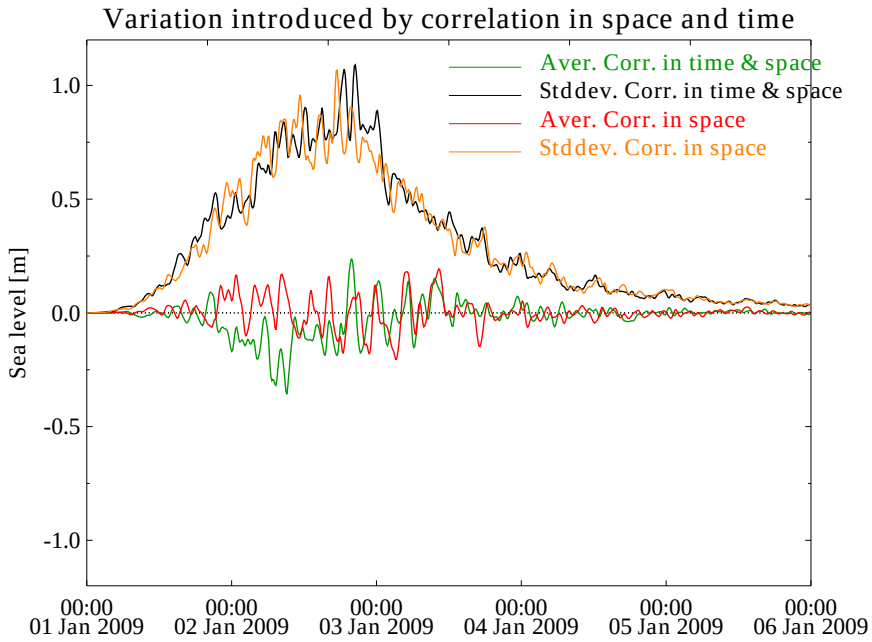

Figure 3.20: Standard deviations of ensemble with spatial correlated noise, in orange and ensemble with both spatially and temporally correlated noise in black. The average deviation from the runs with uncorrelated noise is shown in red for the ensemble with only spatial correlation and green for the ensemble with both spatial and temporal correlation.

3.6 Parameterisation of short term fluctuations as uncorrelated noise

3.6.1 Method

In sections 3.4-3.5 gustiness is approximated by the introduction of noise in the wind forcing, for every time step and grid point. The slowly varying wind field U was uniform in space, as was the standard deviation of the short term fluctuations. In realistic situations this is not the case. In Figure A.2 in Appendix A for instance, we observe wind and gustiness that varies in space. Also, we want to eliminate the ensembles for practical applications. This prompts for a parameterisation of the gustiness effect on storm surges.

To achieve this the wind forcing that has been proposed in section 3.1.1 is replaced. The new wind forcing reads

$$\boldsymbol{u_{aN}}(\boldsymbol{x},t) = \begin{pmatrix} -\sin\phi & \cos\phi \\ -\cos\phi & -\sin\phi \end{pmatrix} \begin{pmatrix} \sqrt{U(\boldsymbol{x},t)^2 + \beta\,\sigma_{u'}(\boldsymbol{x},t)^2} \\ 0 \end{pmatrix}. \tag{3.9}$$

The longitudinal wind $U(\boldsymbol{x},t) + u'(\boldsymbol{x},t)$ is replaced by the quadratic addition of the mean wind speed and a factor β times the standard deviation of the longitudinal short term fluctuations. There is no lateral component of the wind in this parameterisation. This representation is convenient for practical applications later on, because both U and $\sigma_{u'}$ are output parameters of atmospheric models that vary in space and time. β is a constant. We use it to tune the results with the new wind forcing to the results with the ensembles.

The idea of the quadratic addition of U and $\sigma_{u'}$ is based on equation (2.11), where the resulting mean stress also is a function of the quadratic addition of mean wind and standard deviations of the short term fluctuations. The longitudinal component in equation (3.9) becomes

$$\sqrt{U(\boldsymbol{x},t)^2 + \beta\,\sigma_{u'}(\boldsymbol{x},t)^2} = U(\boldsymbol{x},t)\sqrt{1+\beta\,\alpha_u^2}, \tag{3.10}$$

where $\alpha_u = \sigma_{u'}/U$ is the ratio of the short term variations and the slowly varying wind speed. It can be recognised from the former experiments. Note that in this parameterisation only the longitudinal standard deviation is used. The lateral standard deviation is assumed to be a factor r times the longitudinal standard deviation. Following Kaimal et al. [1972] we use $r = 0.75$ (see section 2.1.2). We will compare the outcomes of the first experiment in section 3.1 ($\alpha_u = 0.4$, $\alpha_v = 0.3$) with the results of the run of the model with the new parameterisation for the wind forcing. Here we use thus: $\alpha_u = 0.4$. The runs with added correlation are not used in the comparison, because the variation between the different realisations is high and their average does not deflect much from the runs with random noise.

Goal of this experiment is to validate the parameterisation and determine the constant β empirically. The latter is done by means of a test of various values for β, in a way that we obtain the same results with equation (3.9) as the mean of the ensemble with added random noise.

3.6.2 Results

The result of this experiment is shown in Figure 3.21. The ensemble of 50 realisations of the random noise run is shown in orange. Again, the red line denotes the surge level for no noise addition. We tried various values for a β up to two significant figures. It cannot be determined in a continuous domain, since for every value a new run has to be executed. In the run that fits the Monte Carlo experiments best, $\beta = 2.2$. This run is shown in black. It lies in the middle of the 50 realisations with added noise and has the same shape. This parameterisation would thus give a reasonable prediction of the surge.

Also for the other gauges along the coast the parameterisation approaches the results of the random noise runs well. As an example North Shields in England can be seen in Figure 3.22.

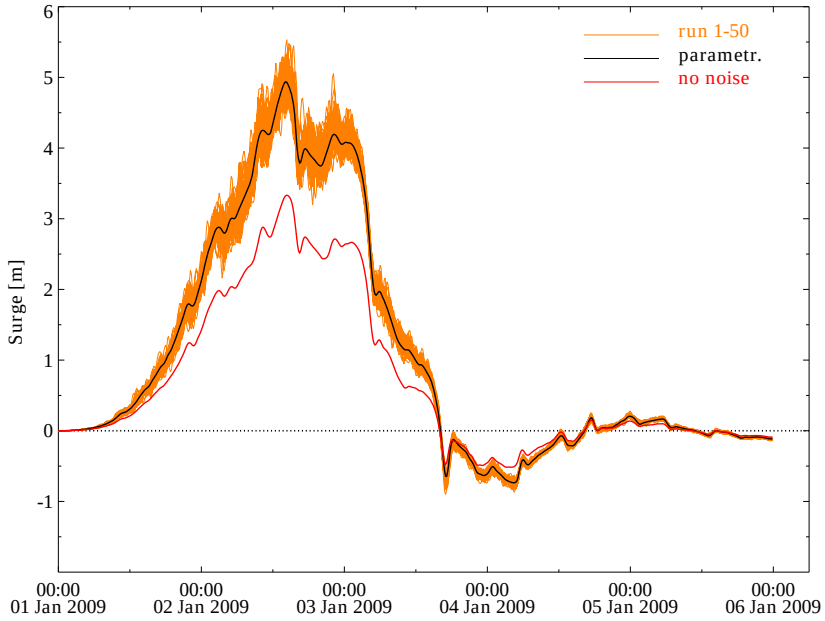

Figure 3.21: Surge in Hoek van Holland of 50 ensemble runs with uncorrelated noise runs in longitudinal and lateral direction: $\alpha_u = 0.4$ and $\alpha_v = 0.3$ (orange lines). The black line gives the surge of the run with the parameterisation, with $\beta = 2.2$. Red line is the no noise run.

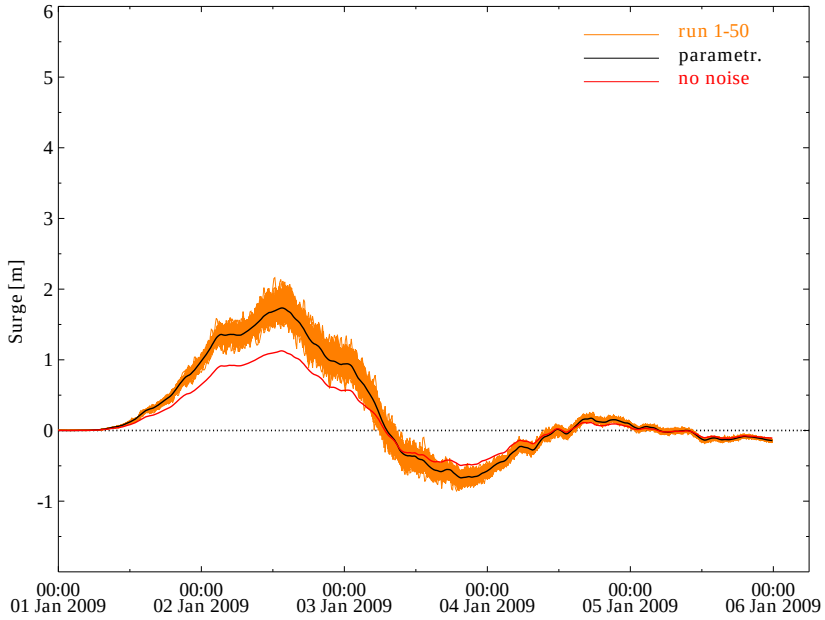

Figure 3.22: Surge in North Shields of 50 ensemble runs with uncorrelated noise runs in longitudinal and lateral direction: $\alpha_u = 0.4$ and $\alpha_v = 0.3$ (orange lines). The black line gives surge of the run with the parameterisation, with $\beta = 2.2$. Red line is the no noise run.

3.6.3 More complicated wind fields

To get more confidence that the parameterisation approaches the effect of gustiness on a storm surge, we assess an experiment with a more complicated wind field. The question is: does the parameterisation also work in cases where mean wind and short term deviation are not uniform in space? Therefore we create a new wind field that is not uniform in space. It is based on the wind fields that we used before in the first Monte Carlo experiment. A schematic map of the wind field is shown in Figure 3.23

We use equations (3.1), (3.2), (3.3) and (3.4) again as wind forcing for the random added noise runs. But now M, ϕ, α_u and α_v are not uniform anymore. In other words the wind speed, wind direction and added noise vary over the domain. They have different values in the different quadrants. First of all

$$\begin{aligned} \alpha_u &= 0.4\, f_\alpha \quad \text{and} \\ \alpha_v &= 0.3\, f_\alpha\,, \end{aligned} \tag{3.11}$$

so the 4/3 ratio of the longitudinal and lateral short term fluctuations remains. Then M, ϕ and f_α vary between the quadrants:

$$\begin{array}{llllll} \text{For latitude} > 56°\text{N} & \text{and longitude} > 2°\text{N} & M = 37.5m/s & \phi = 45° & f_\alpha = 0.4\,, \\ \text{for latitude} < 56°\text{N} & \text{and longitude} > 2°\text{N} & M = 10.0m/s & \phi = 225° & f_\alpha = 1.5\,, \\ \text{for latitude} < 56°\text{N} & \text{and longitude} < 2°\text{N} & M = 12.5m/s & \phi = 180° & f_\alpha = 1.0\,, \\ \text{for latitude} > 56°\text{N} & \text{and longitude} < 2°\text{N} & M = 30.0m/s & \phi = 315° & f_\alpha = 0.8\,. \end{array} \tag{3.12}$$

The procedure for creating the noise stays the same. These values for M, ϕ, α_u and α'_v are also used in equation (3.9) for the new run with parameterisation. The value $\beta = 2.2$ is used again.

The results of an ensemble of 50 realisations with random noise is shown in orange in Figures 3.24 3.25 for gauges Hoek van Holland and North Shields, respectively. The black lines represent the runs with the parameterisation of the short term variations. The result of the no-noise run is represented by a red line.

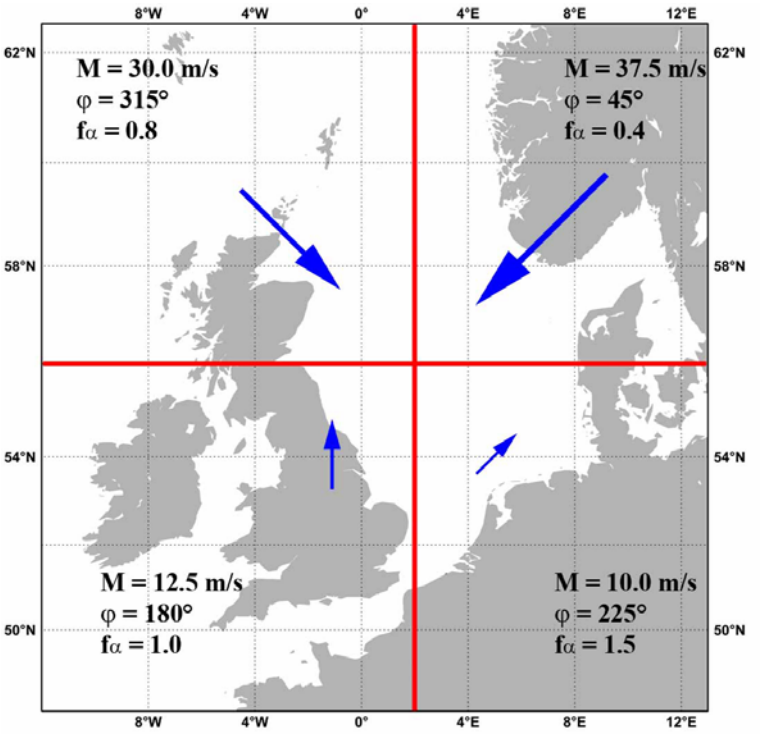

Figure 3.23: Schematic overview of the wind field that is used in experiments to test the parameterisation for gustiness.

The black line deviates from the middle of the orange band. This means that the parameterisation amplifies too little. This effect is quite small though, especially compared to the no-noise run. The parameterisation is considered to approach the Monte Carlo no noise runs relatively well. We keep the parameterisation to investigate realistic cases.

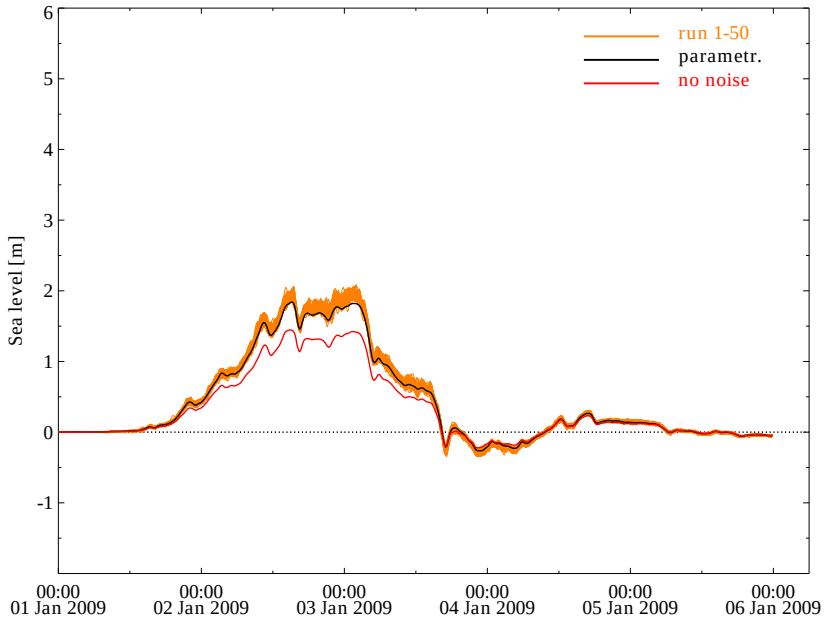

Figure 3.24: Surge in Hoek van Holland of 50 ensemble runs with uncorrelated noise runs in longitudinal and lateral direction: $\alpha_u = 0.4$ and $\alpha_v = 0.3$ (orange lines). The black line gives the surge of the run with the parameterisation, with $\beta = 2.2$. Red line is the no noise run.

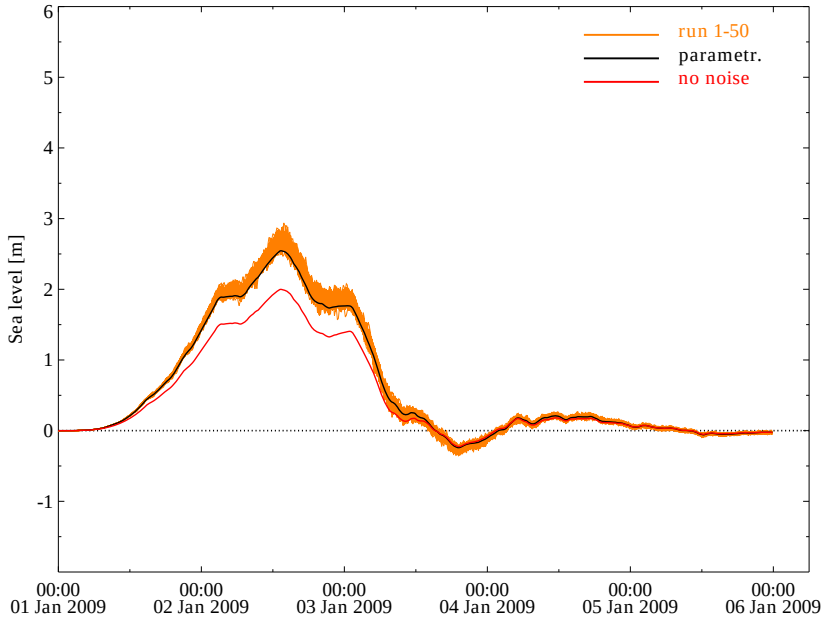

Figure 3.25: Surge in North Shields of 50 ensemble runs with uncorrelated noise runs in longitudinal and lateral direction: $\alpha_u = 0.4$ and $\alpha_v = 0.3$ (orange lines). The black line gives the surge of the run with the parameterisation, with $\beta = 2.2$. Red line is the no noise run.

Chapter 4

Simulating effect of gusts on realistic surges

4.1 Method to generate runs

After the experiments with the simplified and idealised wind fields in chapter 3, we move to realistic storm surge situations. In these situations wind fields and short term wind fluctuations vary in space and time. Also atmospheric pressure variations are included. Thus, it is complicated and unfavourable to carry out Monte Carlo experiments. Therefore we introduced a parameterisation of the effect of gustiness in section 3.6.

One can define the wind forcing of a *traditional* WAQUA/DCSM run with ECMWF input as

$$\boldsymbol{u_{aT}}(\boldsymbol{x},t) = \begin{pmatrix} -\sin\phi_E(\boldsymbol{x},t) & \cos\phi_E(\boldsymbol{x},t) \\ -\cos\phi_E(\boldsymbol{x},t) & -\sin\phi_E(\boldsymbol{x},t) \end{pmatrix} \begin{pmatrix} U_E(\boldsymbol{x},t) \\ 0 \end{pmatrix}, \tag{4.1}$$

where ϕ_E and U_E are wind direction and wind speed from the ECMWF model at location $\boldsymbol{x}$ and time t. In the case where we would like to incorporate gustiness, we replace this forcing of WAQUA/DCSM by another formulation.

For the *new* wind forcing $\boldsymbol{u_{aN}}$ we use the parameterisation that is proposed in equation (3.9). In this way the influence of gustiness on the storm surge is taken into account.

$$\boldsymbol{u_{aN}}(\boldsymbol{x},t) = \begin{pmatrix} -\sin\phi_E(\boldsymbol{x},t) & \cos\phi_E(\boldsymbol{x},t) \\ -\cos\phi_E(\boldsymbol{x},t) & -\sin\phi_E(\boldsymbol{x},t) \end{pmatrix} \begin{pmatrix} \sqrt{U_E(\boldsymbol{x},t)^2 + \beta\sigma_{u',E}(\boldsymbol{x},t)^2} \\ 0 \end{pmatrix}, \tag{4.2}$$

where the parameters ϕ_E, U_E and $\sigma_{u',E}$ are wind direction, wind speed and standard deviations of the longitudinal short term wind fluctuations, obtained from the ECMWF model. Standard deviation $\sigma_{u',E}$ was obtained using equation (2.15). Again we use $\beta = 2.2$.

The wind fields that have been used are forecast runs of the ECMWF model, which are obtained from the Meteorological Archival and Retrieval System (MARS). These runs are carried out twice a day and fields are produced at 3 hour intervals. Because usually the first few hours of the forecast are best predicted, the +3, +6, +9 and +12 forecast fields are used. For the wind and pressure holds that the field is valid right on the time of the forecast. These fields are interpolated in space, towards the WAQUA/DCSM grid. Also linear interpolation in time is done, to obtain fields on the 10 minute time step of WAQUA/DCSM.

The standard deviation of the longitudinal short term fluctuations is obtained from the fields of wind gust (see appendix A for details). In equation (2.15) it is shown that this standard deviation is a function of the wind gust and the wind speed. This wind gust is valid over a certain time interval. In the forecasts of ECMWF this time interval is 3 hours. That is why the wind gust is interpolated in space, but in time the wind gust is taken constant during the interval. The difference in interpolation is illustrated in Figure 4.1. For a wind component it is interpolated linearly in time (blue). The wind gust it is taken constant (red).

Now we have fields of wind, pressure and wind gusts on 10-minutes time intervals. We used fields that range from 1 September 2007 to 1 April 2008. The fields are used to perform two long runs of the storm surge season 2007-2008. One run with the Traditional model, i.e. a run with WAQUA/DCSM that uses the

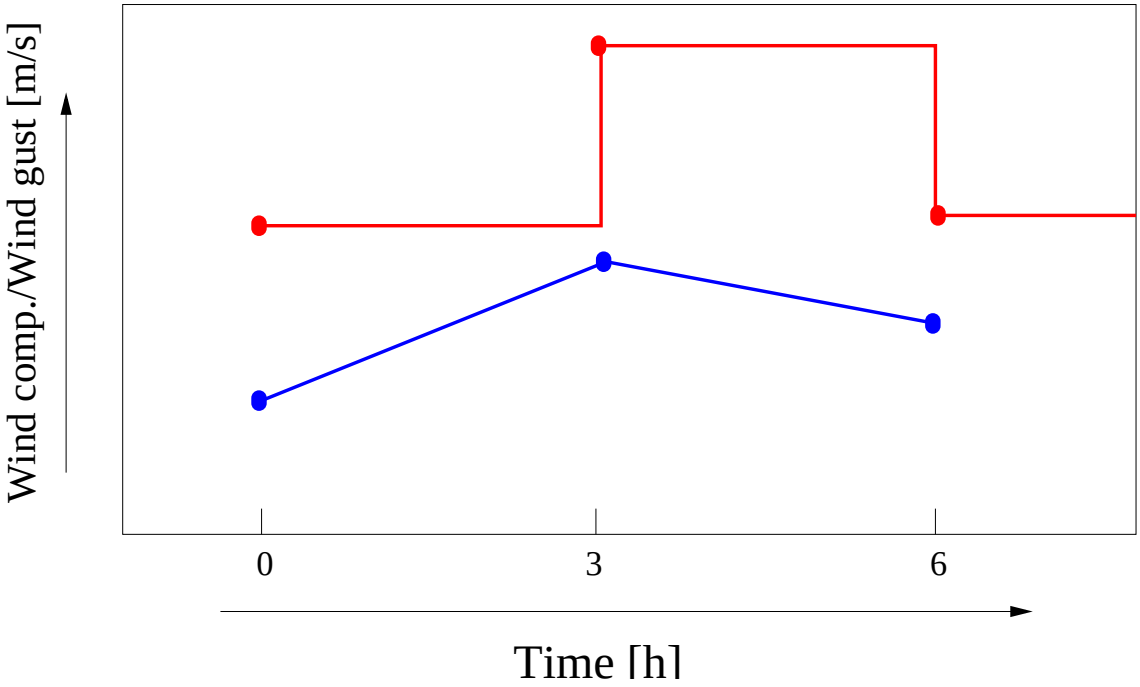

Figure 4.1: Example of interpolation in time of wind components (blue) and wind gust (red) at a grid point.

wind forcing of equation (4.1), and one run with the New model, i.e. a run with WAQUA/DCSM that uses the wind forcing of equation (4.2). From these runs time series are produced in the gauges along the Dutch coast. The two runs are compared to each other and to Observations in the gauges.

Note that here we are comparing the sea level or storm tide which is the addition of the astronomical tide and the surge. First of all three cases of a few days will be picked from the time series to see the qualitative effect of the gustiness on high surges. Later on, the time series will be used to perform statistical experiments (sections 4.3 and 4.4). We remark that the Charnock coefficient β_C (section 2.1.2) is not adjusted for the experiments with the new model. Because of this, we expect that the new model on average will have too high values for positive surges in comparison to the observations. However, we can observe to what extent the addition of gustiness amplifies the results.

4.2 Results of three individual cases

With a parameterisation of short term fluctuations, we take a look at the results of some runs of realistic cases. Here we compare the *traditional* with a *new* run that were described in section 4.1. From runs of storm surge season 2007 - 2008 we selected 3 cases: A large surge at 9 November 2007, a surge on 7 December 2007 and a negative surge in January 2008. They will be presented as time series of the total sea level or storm tide, i.e. the astronomical tide plus the surge. This is done because we will observe different behaviour in the tidal peaks and troughs.

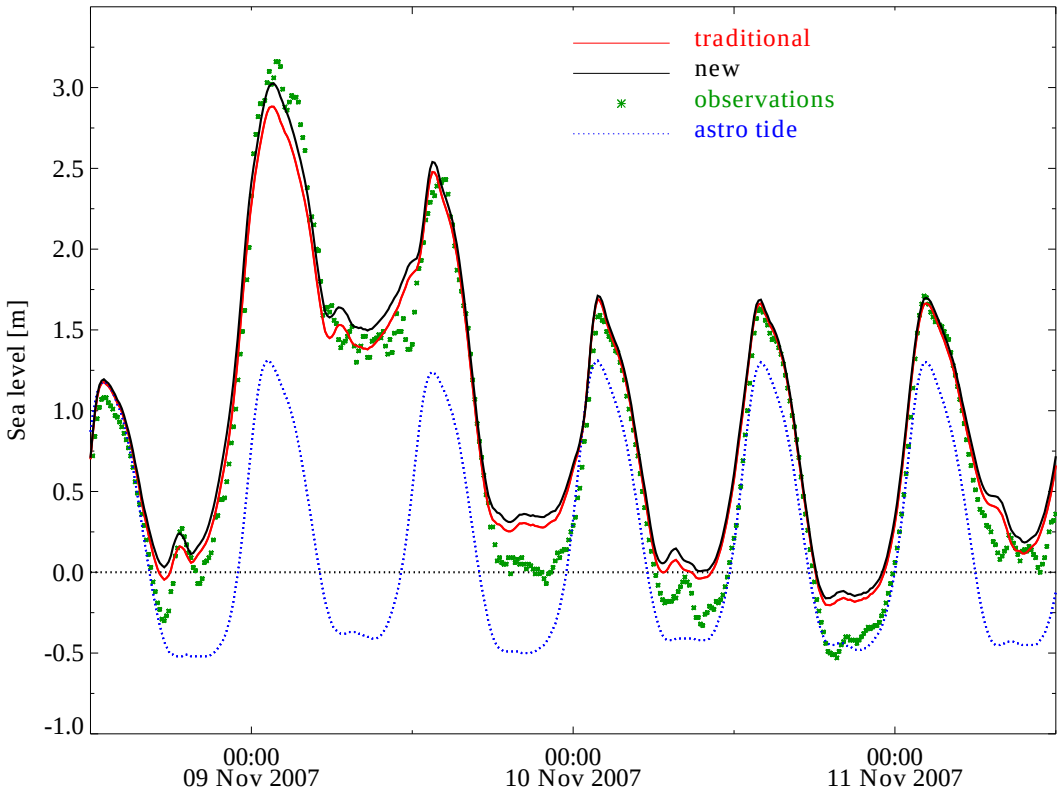

Figure 4.2: Time series at Hoek van Holland of sea level of a realistic case. The red line denotes a run with the traditional model and the black line shows a run with the new model with inclusion of gustiness. Observations are given as green asterisks. The blue dotted line is the astronomical tide.

4.2.1 9 November 2007

In Figure 4.2 we see the case of a big surge on 9 November 2007 at Hoek van Holland. The blue dotted line is the astronomical tide, the green dots are observations of the Hoek van Holland gauge, and the red and black line are the model runs. Here, the red line is a run with the traditional model. The black line is a run with the new model that includes gustiness.

The observations show a surge at 9 November 0 UTC of almost 2 meters. The traditional model underestimates the surge considerably. It is almost half a meter too low on the peak of the tide. The run with inclusion of gustiness in the calculations results into a higher surge. This was expected, since the longitudinal stress on the sea surface is increased. In this case the new model is closer to the observations.

Remarkable is that in the case of the first peak at 0 UTC, the difference between the new run and the traditional run is higher than in the case of the second peak at about 14 UTC. This corresponds also to the

observations, where they lie a lot higher at 0 UTC (in comparison to the red line), than at 14 UTC, where the peak of the red line is on the same level. This shows that, in a this case, the inclusion of gustiness gives a relative rise in the right direction.

Furthermore, we have to emphasise that the low tides are calculated wrong several times in this case, both for the no gustiness run as well as for the gustiness run. We expect that there is another reason for this behaviour than the exclusion of gustiness. We know that WAQUA/DCSM in general has better results for high tide than for low tide.

Some more complications arise with this surge. This surge event is the biggest storm surge since the flooding in 1953. Due to the large surge in Hoek van Holland, the Storm Surge Warning Service (SVSD) decided to close the storm surge barriers along the southern Dutch coast. This was done at 8 November 22 UTC [SVSD, 2007]. Among these closed barriers is also the Maeslantkering, which is close to the gauge of Hoek van Holland. It closed for the first time during a storm surge, since the Maeslantkering was put into service in 1997. It opened again at 18 UTC the next day.

One expects that, due to the piling up of water against the storm surge barrier, the surge is raised a few decimetres. One can thus argue whether the observations would be so high if the barrier would have stayed open. In Den Helder though, there is no storm surge barrier. The detail of the big surge is shown in Figure 4.3. Here we also see that observations are higher than both model runs. The new run is higher than the traditional run.

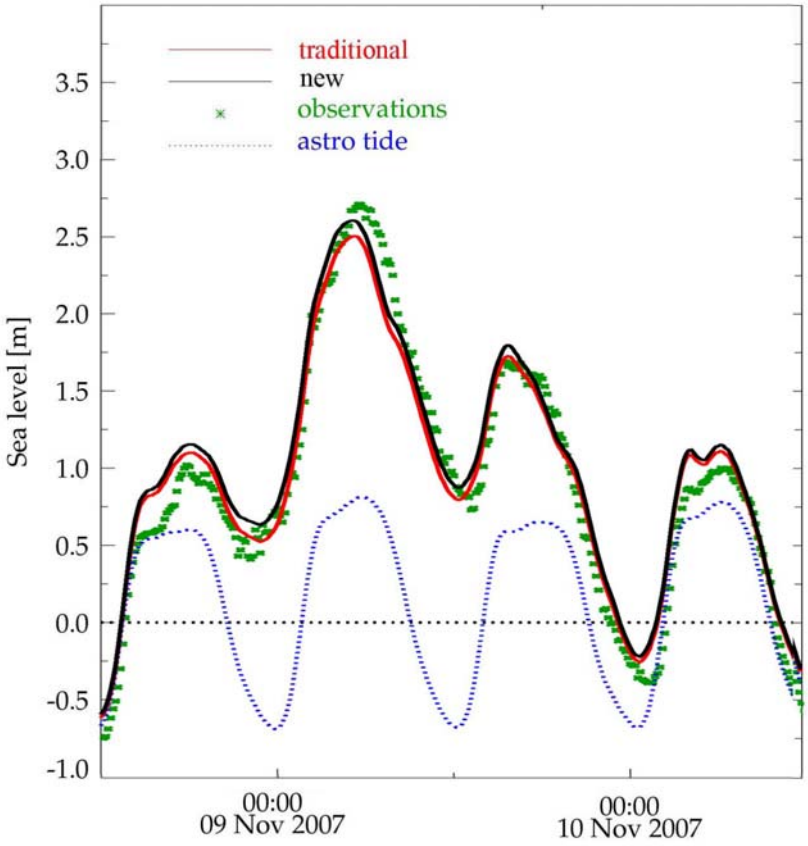

Figure 4.3: Detail of the same event as in Figure 4.2, but for Den Helder.

4.2.2 7 December 2007

An example of a case where the the run with inclusion of gustiness is not improving the result is shown in Figure 4.4. A surge is found of about 1 meter at 7 and 8 December 2007. The traditional run is already close to the observations each time. At the peak on 7 December 12 UTC, the difference between the new model and the traditional model is highest. But here the observations are closest to the traditional model. Apparently, the effect of gustiness was lower than the new model predicted. The peak at 8 December 14 UTC is also not enhanced in the right way. Both models are too low in comparison to the observations, also the new one with gustiness.

The peak at 8 December 0 UTC is better. Both the observations as well as the new model run are higher than the traditional model run. The differences between the new model and the traditional model are small in this case, so it is hard to tell whether the new model improves results.

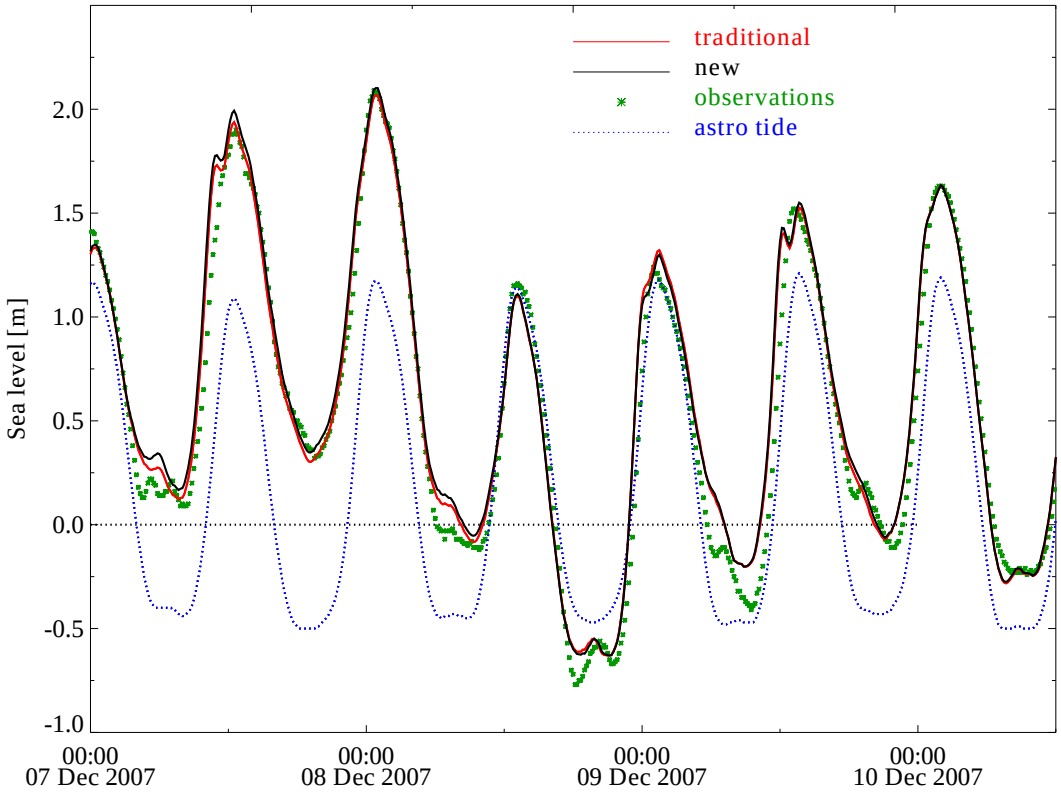

Figure 4.4: Time series at Hoek van Holland of sea level of a realistic case. The red line denotes a run with the traditional model and the black line shows a run with the new model with inclusion of gustiness. Observations are given as green asterisks. The blue dotted line is the astronomical tide.

4.2.3 January 2008

The case of early January 2008 is chosen to show the impact at a negative surge. In the negative surge case especially low tide is important e.g. for shipping in harbours and estuaries. In this case we see that for several days the the low tide is not predicted well (Figure 4.5): the model run is too high. The new run, with gustiness included, yields results that are closer to the observations at low tide. Still, the difference between observations and the new run is large. We have take into account here that WAQUA/DCSM generally is less capable to predict low tides and negative surges well than high tides and positive surges. So no inclusion of gustiness is not the only reason why the traditional model is wrong here.

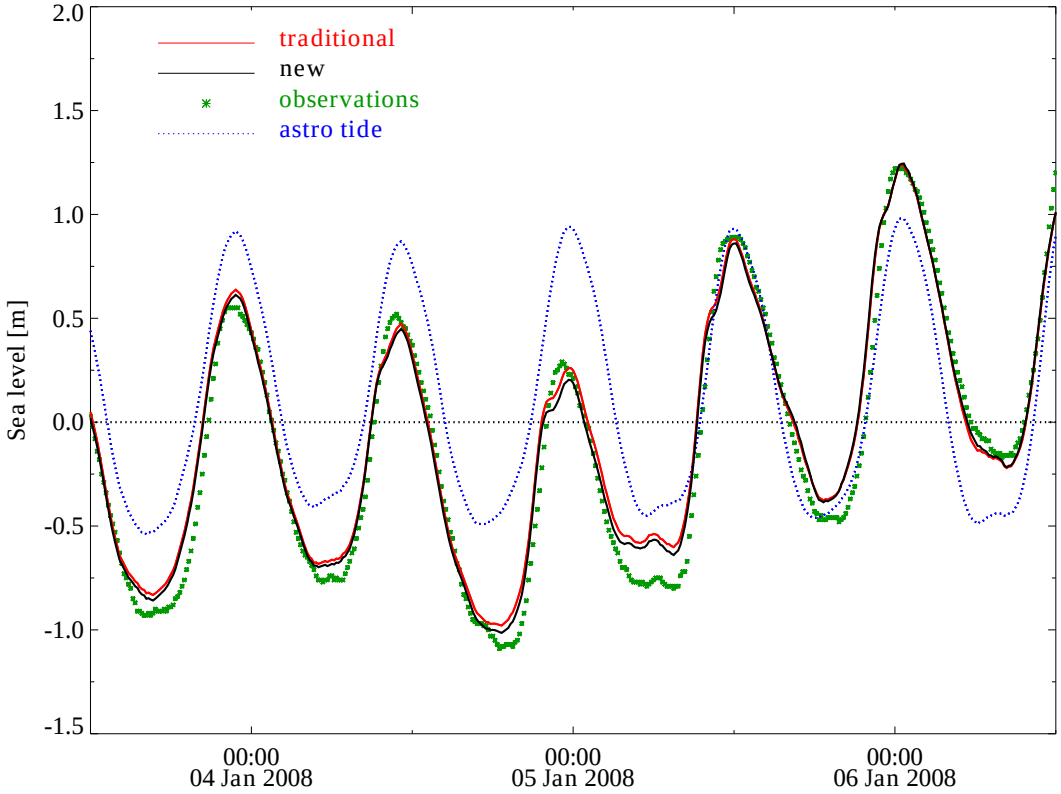

Figure 4.5: Time series at Hoek van Holland of sea level of a realistic case. The red line denotes a run with the traditional model and the black line shows a run with the new model with inclusion of gustiness. Observations are given as green asterisks. The blue dotted line is the astronomical tide.

From these three cases we can not deduce whether the new model yields better or worse results than the traditional model. In some cases the result is moved in the direction of the observations, in others not. We suspect that there will also be relatively large errors in the models due to other circumstances than gustiness, e.g. errors in meteorological output of the ECMWF model. Although differences between the new and traditional model are sometimes small, we found that the addition of gustiness does change the result.

4.3 Method to analyse runs

To study the effect of gustiness on a storm surge in a statistical way, the long time series of the storm surge season 1 September 2007 - 1 April 2008 of the traditional model and the new model are used. How these time series are created is described in section 4.1. Again, the traditional and new run are compared to observations, along the Dutch coast at the five gauges: Vlissingen, Hoek van Holland, Den Helder, Harlingen, and Delfzijl (Figure 2.7).

Because of tide-surge interaction [Horsburgh and Wilson, 2007] maxima and minima of the surge tide do not always occur at the same time as the maxima and minima of the astronomical tide. This is why the skew surge is a quantity that is needed to compare the models to observations (see Figure 1.1). Three time series of skew surges are created for the traditional model, new model and observations. The three datasets contain for every gauge about 400 high and low tide skew surge levels.

We will call the skew surge at the high and low tide for new model H_N. For the traditional model it is called H_T and for the observations it is called H_O. What will be of interest to verify the influence of gustiness on a storm surge? First of all we are interested in the error of the traditional WAQUA/DCSM run, which is the difference between the modelled skew surge without gustiness and the observations

$$\text{ERROR} = H_T - H_O. \tag{4.3}$$

We use the difference between the new model and the traditional model as a measure for the amount of gustiness that has affected the skew surge,

$$\text{AMOUNTG} = H_N - H_T. \tag{4.4}$$

We investigate whether ERROR is correlated to AMOUNTG. If a correlation exists, it supports a conclusion that gustiness affects the surge. The high tide and low tide data sets are investigated separately.

4.4 Results of analysis

Figure 4.6 shows how the the observations correspond to the model outcomes for high and low tide separately. Here, the modelled skew surge levels H_T (red crosses) and H_N (black crosses) are plotted against the observed skew surge levels H_O. The blue line gives the ideal result, i.e. levels of the model equal those of the observations.

We see that the models correspond well to the observations; the crosses are close to the blue line. Differences between the traditional and new model are not judged easily. In case of positive surges, the enhanced run gives often a higher surge, i.e. the black cross lies above the corresponding red cross. Negative surges are more negative for the new model run.

	Traditional model				New model			
	High tide		Low tide		High tide		Low tide	
Gauge	Corr.	χ^2-err.	Corr.	χ^2-err.	Corr.	χ^2-err.	Corr.	χ^2-err.
Vlissingen	0.943	49.1	0.967	31.2	0.942	55.8	0.965	32.9
Hoek van Holland	0.961	31.9	0.962	61.9	0.959	32.0	0.961	72.8
Den Helder	0.968	41.3	0.971	51.5	0.966	45.4	0.971	56.1
Harlingen	0.973	32.7	0.963	69.3	0.971	37.2	0.963	79.5
Delfzijl	0.964	30.2	0.967	85.5	0.963	30.8	0.967	86.0

Table 4.1: Correlation and chi-squared error, when comparing the output of the two models to observations.

To find out about the accuracy of the runs, the correlation between observations and model results is given in table 4.1. Also Chi-squared errors from the blue line are given. It turns out that all correlations differ little. Chi-squared errors are higher for the new model run compared to the traditional model. This means that the new model run does not come closer to the observations than the traditional run. This is understandable,

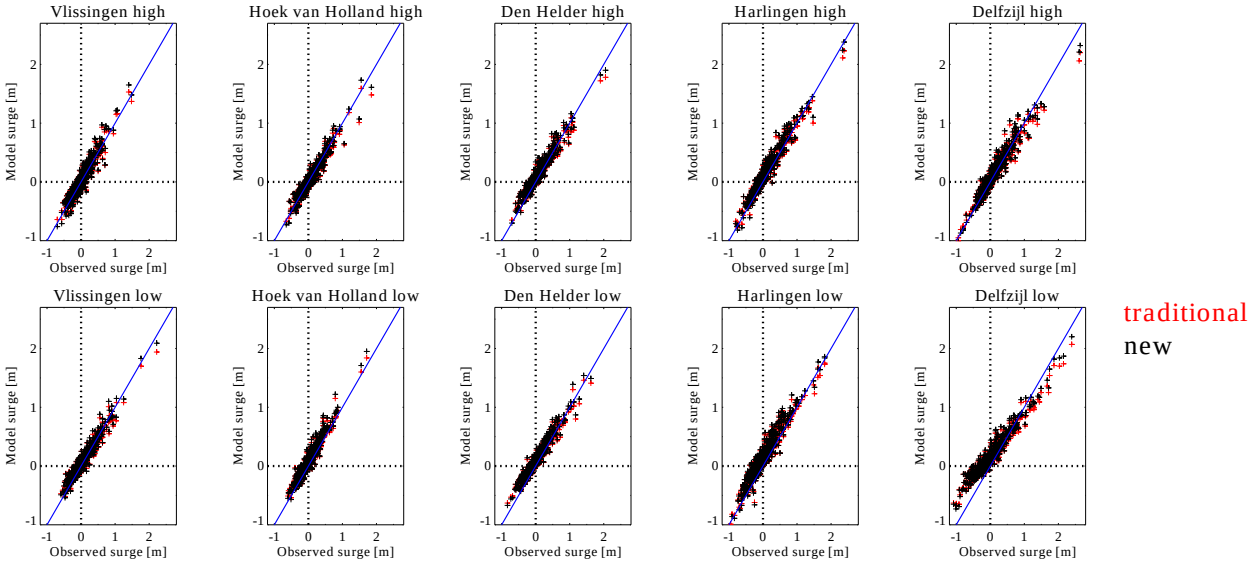

Figure 4.6: Skew surge of observations H_O versus skew surge of the traditional model H_T (red) and the new model with parameterised gustiness H_N (black).

because WAQUA is tuned via the Charnock coefficient, in a way that the model outcomes come closest to observations. When now forcing is changed due to gustiness in the new model, it is not surprising that the chi-squared errors increase. For a better correspondence to the observations the Charnock coefficient should be adjusted in the new model.

Next, we would like to know whether a high (negative) correlation exits between ERROR and AMOUNTG. That would indicate that the addition of explicit gustiness is significant and explains part of the error of WAQUA/DCSM. When plotting ERROR versus AMOUNTG we would find a negative slope, since a high positive addition due to gustiness would correspond to a traditional model that is too low compared to observations (i.e. negative ERROR) and a low positive addition would correspond to a traditional model that is too high (or less low) compared to observations. Plots for all stations at high and low tide are shown in Figure 4.7. In red are the cases with positive skew surge and in green are the cases with a negative skew surge.

No clear negative relation can be observed visually in the data sets presented here, apart from Delfzijl low tide and Den Helder low tide. However, as we will see later on, this stronger negative correlation does not indicate a large influence of gustiness. It shows a strong relation between the error at Den Helder and Delfzijl and the skew surge itself, which in turn is correlated to AMOUNTG. The main conclusion we have to draw here is, that in the observations there is too little evidence to conclude that part of the error can be explained by the addition of a parameterisation for gustiness to a model.

The same conclusion can be drawn when we consider correlations and corresponding significant levels of the error and difference between the new and traditional run in table 4.2. Correlation is always near zero, only in Den Helder and Delfzijl at low tide a larger negative correlation is found. In most cases the correlations are statistically significant (the significant level < 0.05), because so many data poins are used.

One can observe in Figure 4.7 that the error of the the model is large compared to the effect of gustiness. The range of error of the traditional model is in the order of 50 centimetres and the maximum addition due to gustiness is only 10 centimetres. This means that before the effect of gustiness will be important in storm surge forecasting, errors due to other effects, e.g. errors in the meteorological input in the model or bathymetry that is used in the model, have to be decreased first.

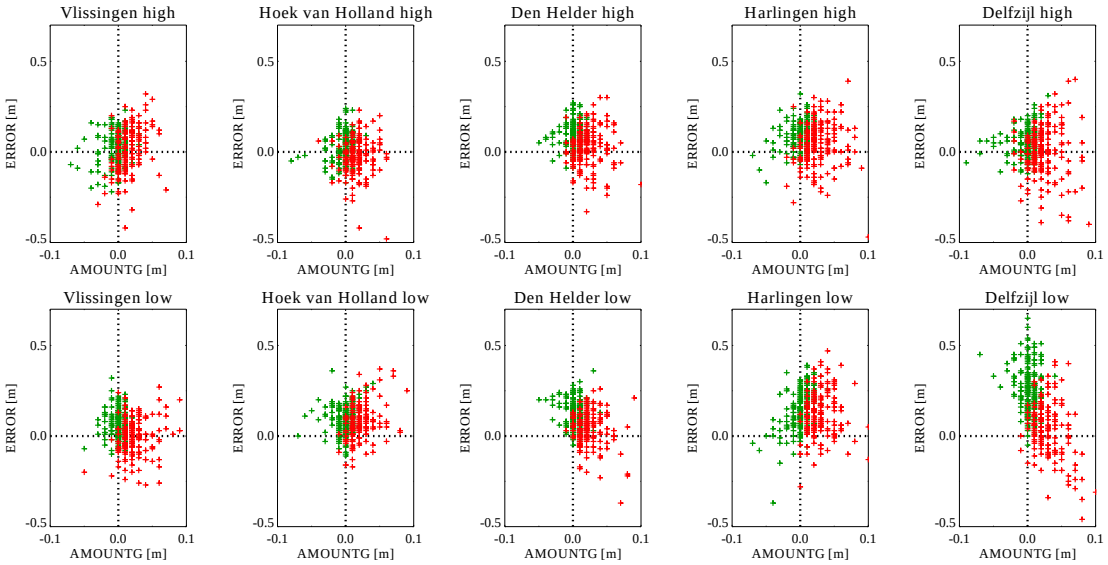

Figure 4.7: Error of WAQUA/DCSM versus the amount of gustiness that has affected the skew surge, which is the difference between the new model with parameterisation and the traditional model: AMOUNTG= $H_N - H_T$. Red crosses are observed positive skew surges and green crosses are observed negative skew surges.

	High tide		Low tide	
Gauge	Corr.	Signif.	Corr.	Signif.
Vlissingen	0.196	< 0.01	-0.190	< 0.01
Hoek van Holland	-0.115	0.02	0.138	< 0.01
Den Helder	-0.188	< 0.01	-0.355	< 0.01
Harlingen	-0.087	0.08	-0.001	0.98
Delfzijl	-0.158	< 0.01	-0.617	< 0.01

Table 4.2: Correlation and signifecant levels (two-tailed) of between ERROR and AMOUNTG.

Figure 4.7 suggests that the addition of gustiness has a seizable impact on the low tide surge in Den Helder and Delfzijl. However, a more evident explanation can be found in the surges themselves. As can be seen in Figure 4.8, the error of the model is also strongly correlated to the skew surge H_T itself of the traditional model in Delfzijl at low tide, and in Den Helder at low tide to a lesser extend. The similarity with the results in Figure 4.7 is remarkable. This problem of WAQUA/DCSM with Delfzijl and Den Helder influences the result. We conclude that in this situation AMOUNTG is correlated to the skew surge of the model H_T, and a strong negative correlation between surge H_T and ERROR leads to the obtained result.

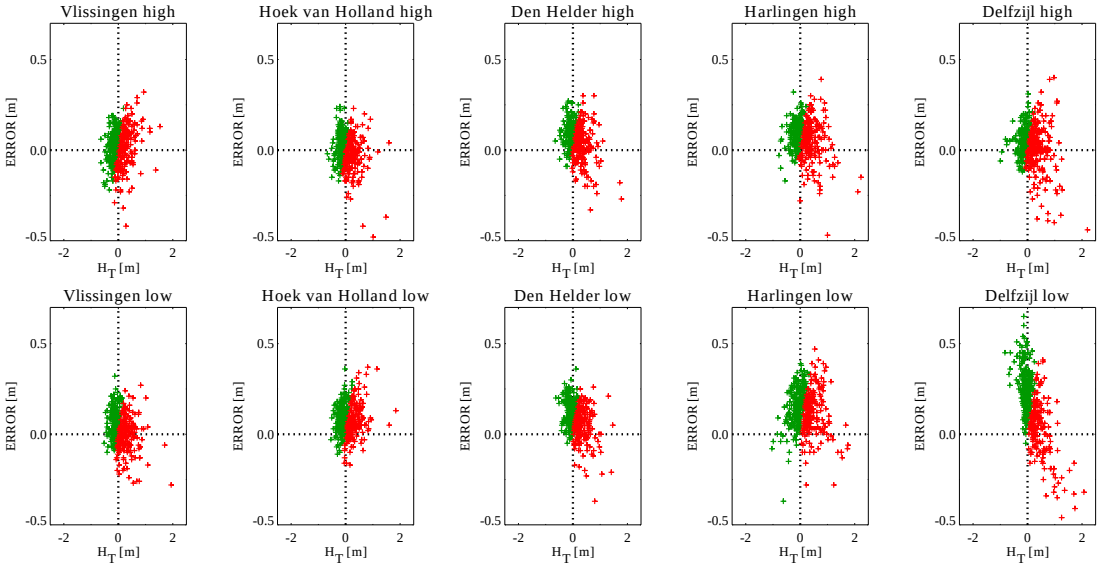

Figure 4.8: Error of WAQUA/DCSM versus the surge of the traditional model H_T. Red crosses are observed positive skew surges and green crosses are observed negative skew surges.

4.5 Experiments with increased β

The same expriments were repeated for a new model with a higher β in equation (4.2). This is done to study the enhancement of the impact of gustiness. We take a value $\beta = 5.0$. Figure 4.9 shows again the ERROR of the traditional model versus AMOUNTG, analogous to Figure 4.7. The range of the AMOUNTG is larger, since the impact of gustiness in increased, but the conclusions are the same as before. In fact, Figures 4.9 and 4.7 have a similar shape.

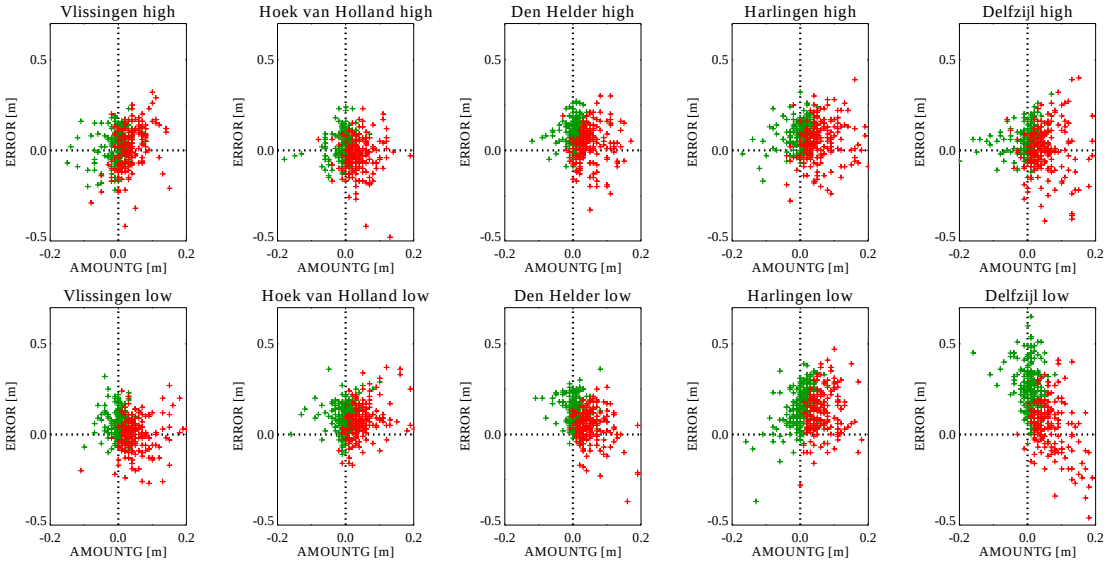

Figure 4.9: Error of WAQUA/DCSM versus the amount of gustiness that has affected the skew surge, which is the difference between the new model with parameterisation and the traditional model: AMOUNTG= $H_N - H_T$. Red crosses are observed positive skew surges and green crosses are observed negative skew surges. The value for β is increased to 5.0.

Chapter 5

Discussion: Is gustiness important?

In this study we included gustiness explicitly in the driving forces of WAQUA/DCSM, via a parameterisation that is presented in section 3.6. In storm surge models the mean effect of gustiness is already taken into account. This is done through the Charnock coefficient that is tuned when the model is calibrated with observations along the coasts. When we now increase the stress due to the addition of explicit gustiness, one should retune the model to obtain results that best fit the observations. This was not done in this study so it is not surprising that initially the total error of the new model increases with respect to observations, as is found in section 4.4.

But in the same section we observed that there is no correlation between the error of the traditional model with respect to observations and the difference between the traditional and new model output. This indicates that the addition of explicit gustiness is not important. Thus, the answer to the second question that is asked in the introduction is: the explained error due to the explicit addition of gustiness is small compared to other errors in WAQUA/DCSM.

This can also clearly be seen in Figure 4.7, where on the x-axis is given the addition to the skew surge due to explicit gustiness, and on the y-axis the error of the traditional model with respect to the observations. When we consider the range of these axes, we see that the influence of gustiness is maximum 10 centimetres, whereas the error of the traditional model could be as high as half a meter. No linear relation can be found.

The impact of gustiness can be adjusted by the constant β in the parameterisation. When we take $\beta = 2.2$, the parameterisation corresponds best to the Monte Carlo experiments. When we increase β the effect of gustiness will be higher. Also in the experiments with a higher β we see the same results, that there is no relation between the error and the added skew surge due to explicit gustiness.

Can we thus conclude that there is no need to incorporate explicit gustiness in numerical storm surge models at the moment? The results in section 4.4 suggest it. But before we do this we have to consider all steps that are taken before this final experiment. Are the Monte Carlo experiments performed correctly? Is the parameterisation correct?

In the Monte Carlo experiments the time scale of the fluctuations is 10 minutes, which is the time step of WAQUA/DCSM. One might suggest that this is long for short term variations. But according to the theory in section 2.1.2 this should not be important. What determines the extra stress on the sea surface is the standard deviation of the short term variation. This is not influenced by the time scale of the fluctuations. Also an experiment is performed with a smaller time step of 1 minute. This did not influence the results.

Furthermore, we note that the Monte Carlo experiments use very simplified and exceptional wind fields. The spatial extent and the duration of the storm make it an exceptionally severe storm case. The effect of gustiness in the experiments is uniform in space, i.e. the standard deviation of the added short term variation is constant in space, leading to an enhancement of the stress that is uniform in space. In realistic situations gustiness fields are not uniform (see Figure A.2). It is assumed that the local enhancement of the stress due to gustiness is the same as in the case where we have this same gustiness value in a uniform field.

In the new model the effect of wind gusts is parameterised. The parameterisation is based on the results of the first Monte Carlo experiment. In a verification of the parameterisation, in section 3.6.3, a run with parameterised gustiness deviates relatively little from the ensemble realisations, when it is compared to the no-noise run. So, we believe that the parameterisation shows the right effect that was found in the Monte

Carlo experiments.

We thus conclude that the effect of an explicit incorporation of gustiness in the model is small compared to other errors that already exist in the model. These have to be reduced before explicit gustiness becomes important. The errors that we find now in the output of WAQUA/DCSM can have various causes. Here, we will sum up some properties that can be improved on contemporary storm surge models.

What causes the highest error in storm surge predictions are errors in the input data. This input data comes from meteorological models like HiRLAM or ECMWF. The fields of pressure and surface wind contain considerable errors compared to reality. As a consequence, also the output of WAQUA/DCSM has a higher error. The development of the meteorological models will eventually reduce errors in the storm surge models.

A major field of research is the air-sea interaction on an elementary level: the drag relation. The manner to determine the value of the Charnock coefficient is not yet undisputed. As is shown before, in WAQUA/DCSM it is taken constant, but it is likely that it is a function of several parameters. Powell et al. [2003] argue that it is a function of the wind speed. For high wind speeds the drag coefficient is reduced. In other studies such as Donelan et al. [1993], the wave state is important to the determination of the drag coefficient. Steep waves generate more drag than more smooth waves.

Most storm surge models are 2-D shallow water models. In these models 3-D effects of the fluid are not taken into account. Inter-comparisons show that differences are found between a 2-D and a 3-D model [Weisberg and Zheng, 2008]. In the 2-D model bottom stress is often overestimated. This results in a change in the dynamical balances and necessitates unrealistic parameterisations of surface stress and other techniques for calibration. Weisberg and Zheng [2008] prefer 3-D models over 2-D models for simulation of storm surges in complex coastal topography.

Chapter 6

Conclusions

The focus of this study is on the influence of gustiness on sea surface heights in storm surge situations. Short term fluctuations of the wind result in a positive contribution to the stress on the sea surface. We set up several experiments with idealised and realistic cases to address the following specific questions. Can part of the error of a storm surge model be explained by the varying effect of short term fluctuations? How big is this part of the error, when we add the effect of short term fluctuations explicitly to the model, compared to other errors that are introduced in the system, e.g. by errors in atmospherical input and errors in bathymetry?

In this study the storm surge model WAQUA/DCSM is used. We examined the error of WAQUA/DCSM relative to observations of gauges along the Dutch coast. To include gustiness explicitly the following steps were taken: Monte Carlo experiments are performed with simple and idealised wind fields to explore the effects of short term variations in the wind; a parameterisation for these effects is developed and tested. The new model that is applied on realistic situations uses this parameterisation. The new model is compared to the traditional model that does not include gustiness explicitly in experiments with realistic wind and pressure input.

In the Monte Carlo experiments we studied the effect of gustiness on the sea surface height with an idealised wind field, where short term variations are added to a uniform wind. It was investigated in a statistical manner; ensembles of 50 realisations were performed. Different wind angles and different noise characteristics were studied. We conclude that the surge is amplified by the addition of noise. When the amount of noise is increased, the amplification gets stronger. For reasonable realistic wind variations this amplification of the surge can be about 10 per cent. When we use spatially and temporally correlated noise, an increase of the variability of the surge between different realisations is found. But concerning the average amplification, these experiments are in agreement with the experiment of the random noise run.

For the new model with an explicit addition of gustiness we adjusted the wind forcing. The wind speed was quadratically added to the gustiness $\sigma_{u'}$. In this parameterisation the relative impact of gustiness is specified with a constant β. The best value in the present setting is 2.2. This was determined by in empirical comparisons to the outcomes of the Monte Carlo experiments that were performed before.

Three realistic surge cases are selected from the storm surge season 2007 - 2008, to further test the new model. In these experiments results of a run with the new model is compared to results of a traditional model run (without explicit gustiness) and observations in gauges along the Dutch coast. At several points the new model run differs from the traditional model run. The change did not always correspond to the error of the traditional model from the observations. From these separate cases, we cannot conclude that this parameterisation improves the outcomes of the model.

From the analysis of a long run of season 2007 - 2008 we conclude the following. As expected, in the new model run gustiness amplifies a surge. Furthermore, we demonstrated that the error of the traditional model with respect to the observations is not clearly correlated to the amplification due to gustiness. The effect of the addition of explicit gustiness on surges is small compared to the error of the traditional model (about 5 times smaller). So we conclude that, at the moment for WAQUA/DCSM, it is not needed to incorporate effect of explicit gustiness on surges. The error of storm surge models will be reduced in the future, by the improvement in meteorological input for the storm surge models among others. When the error of the model is far smaller, it can be useful to investigate the effect of the addition of explicit gustiness on surges again.

Gustiness could be important in other domains, but for the North Sea the effect on surges is far too diffuse to find an improvement.

Chapter 7

Acknowledgements

It is always pleasant to work on a subject that interests many people and is of great importance. A storm surge is a subject like this. In the Netherlands there has always been a tradition of living from the sea and fighting against it. Tradesmen and fishermen went on their ships to bring their community wealth and success. However, various big disasters occurred, where land was flooded and many people died.

Over time the skills of the Dutch to fight water improved. They built dikes, drained pieces of lakes and expanded international vocabulary by the word 'polder'. Also on a scientific level is worked on the understanding of and making society resistant against storm surges. Committee Lorentz calculated effects of a closure dam of the Zuiderzee on tidal resonance and surge heights. Storm surges have recently become a momentous subject again, due to climate change and the foreseen rising of the sea level. In debates about this subject measures like heightening the dikes and establishing more space for water in rivers are mentioned.

For me it has been interesting to do my graduation thesis at KNMI, which has an important role in the debates above. I have experienced how knowledge, on which policy is based, is acquired in a scientific way. Also, it was nice to see the importance of operational work (forecasts) and the collaboration with other social/governmental organisations. Motivating was the JONSMOD 2010 conference in Delft, where I had the opportunity to present my work. The internship at KNMI has been a valuable completion to studying at the University.

During this study I have been supervised by Hans de Vries from KNMI and Huib de Swart from University Utrecht. I would like to thank them for all time and effort that they put into the work. It has been pleasant and instructive to work together. We had many nice meetings where I got a view in the scientific world. They helped me to improve the results of my work every time again.

Hans supervised me on KNMI. First of all the idea for this subject is his. We had daily conversations about the progress of the study. He also helped me with all trouble that I could have with the Linux workstation. At (virtually) any time of day I could walk into his office and ask any burning question. Often Hans came up with new ideas and improvements.

Huib had another role as supervisor from the University. We had meetings every two weeks to talk about the progression of the study, together or with the three of us. What was nice from these meetings was that we always did a step back and tried get an overview. Why are we doing this? Is the theory correct? Huib came up with many suggestions in these meetings and I was always motivated afterwards to carry on and investigate more.

Furthermore I would like to thank colleagues at KNMI. The atmosphere has always been good and everybody was willing to make time for me for some advice or help. Two names I would like to mention in particular: Kees Kok I thank for his interest in my work. We had some good conversations. And then there is Niels Zweers, my roommate. Apart from his immense helpfulness, he made my time as a temporary KNMI'er very diverting.

24-12-2010, Utrecht

Appendix A

Wind gust and gustiness

In this appendix we will explain more about the term wind gust, as well as the link between wind gust and gustiness, that is introduced in section 2.1.2. This is needed because atmospherical models such as HiRLAM and ECMWF do not directly produce a standard deviation for longitudinal short term fluctuations (gustiness), but only a wind gust, which is related to the standard deviation.

Wind gust is not consistently defined:

- *A sudden strong rush of wind* (Oxford dictionary).
- *The maximum of the wind averaged over three-second intervals* [WMO].
- *The maximum three-second wind speed forecast to occur within a 2-minute interval at a height of 10 meters. Wind gust forecasts are valid at the top of the indicated hour* [NOAA].

A noticeable term in the definitions of NOAA and WMO is the three-second interval of the samples of the wind. This interval is explicitly chosen and has great impact on the value of wind gusts. A fast response system will measure higher wind gusts than slower response systems. To get a uniform definition, it is chosen to use three-second wind speed.

Furthermore, it is clear that the wind gust is the product of the high frequent variations of the wind. Of interest for the impact of a storm, are the extremes in the wind speed. So, emphasis is on the maximum in the wind speed over a time interval. This interval is not consistently used. For gusts defined by NOAA two-minute time intervals will be considered. In the definition of WMO it is not prescribed, and is not three seconds, as the WMO-definition might be misinterpreted. ECMWF uses in its forecasts of the atmospheric model, a time interval 'since the last post-processing time' [Beljaars et al., 2001], which is three hours in this study. One has to conclude that a forecast of gust by NOAA or ECMWF can have two quite different values. Since we have used wind gust data from ECMWF in this study the definition used here will be:

- *The maximum three-second wind speed to occur within a 3 hour interval at a height of 10 meters.*

In Figure A.1 a sketch of an example of a time series of the wind is shown. The maximum speed of the longitudinal wind is shown with the red arrow. We have seen that short term fluctuations are approximately normally distributed, so a histogram of the time series might look something like the right panel in Figure A.1. We assumed that the mean wind is not varying in the time interval. By definition, the value for the wind gust is on the extreme right side of the distribution.

The definition of wind gust allows us to *measure* a wind gust. In atmospheric models it is needed to *predict* a wind gust as well. This is where the standard deviation of the longitudinal short term fluctuations (gustiness) comes in. It is defined in equation (2.10). The model uses this standard deviation to make a prediction of the wind gust. When for instance the standard deviation in Figure A.1 would be larger, the maximum will most probably also be higher. Thus the stochastic characteristics of short term fluctuations are used to make a prediction of the wind gust.

In numerical atmospheric forecast models, the standard deviation of the short term fluctuating wind components can be estimated by using Monin-Obukhov similarity theory [Panofsky et al., 1977].

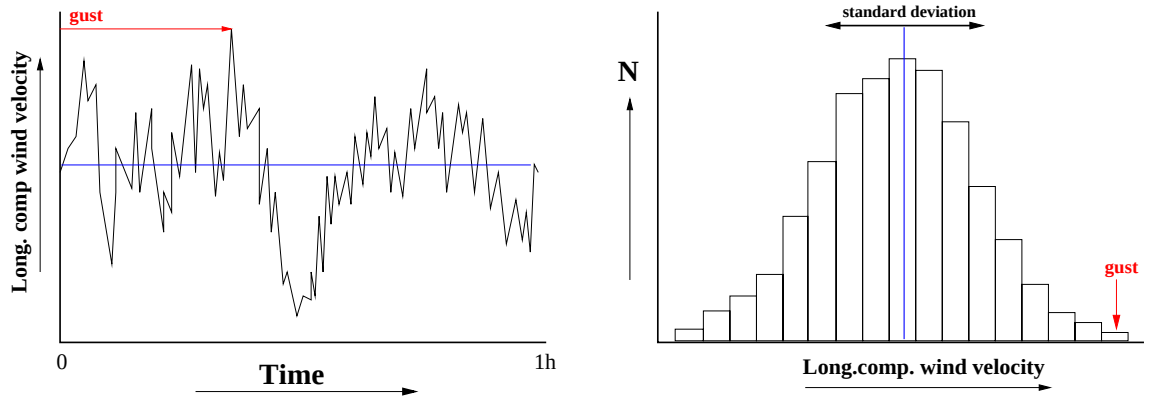

Figure A.1: Drawing of a time series of wind in the left panel, with mean (blue line) and wind gust (red arrow). A histogram of the time series is shown in the right panel. Again mean, standard deviation and wind gust are indicated.

The probability P that the measured wind gust in a time period T exceeds a value G, is a function of the distribution of the wind (mean wind speed U and longitudinal standard deviation σ_u) and the characteristic time scale of short term deviations τ. Characteristic time scales for short term deviations can be found again from the spectra of Kaimal et al. When imposing a value for P, a border value can be calculated [Beljaars, 1987], [Wichers Schreur and Geertsema, 2006].

$$G = U + g\,\sigma_{u'}, \tag{A.1}$$

$$g = \left(2\ln\left(\frac{T}{\tau} \frac{1}{\sqrt{2\pi}\ln(\frac{1}{1-P})} \right) \right)^{\frac{1}{2}}. \tag{A.2}$$

The resulting value G can be interpreted as a prediction for the wind gust, with an exceedance probability P. $\sigma_{u'}$ is the standard deviation of the longitudinal short term fluctuations (gustiness). In the ECMWF model, an exceedance probability of 25% and a time period T of 3 hours is used. It follows then that $g = 2.93$.

An example of a predicted 10 meter wind gust field is shown in Figure A.2. Gust values are obviously higher than the mean wind values. Furthermore, the wind gust is a little less affected by coast lines than the mean wind.

In this study, the computation of wind gust and standard deviation of short term motion will be used the other way around. We are interested in the extra stress that is exerted on the water by the short term motion. So we are interested in the standard deviations of the wind components. The wind gust is an operational output parameter of ECMWF, from which the longitudinal standard deviation will be deduced.

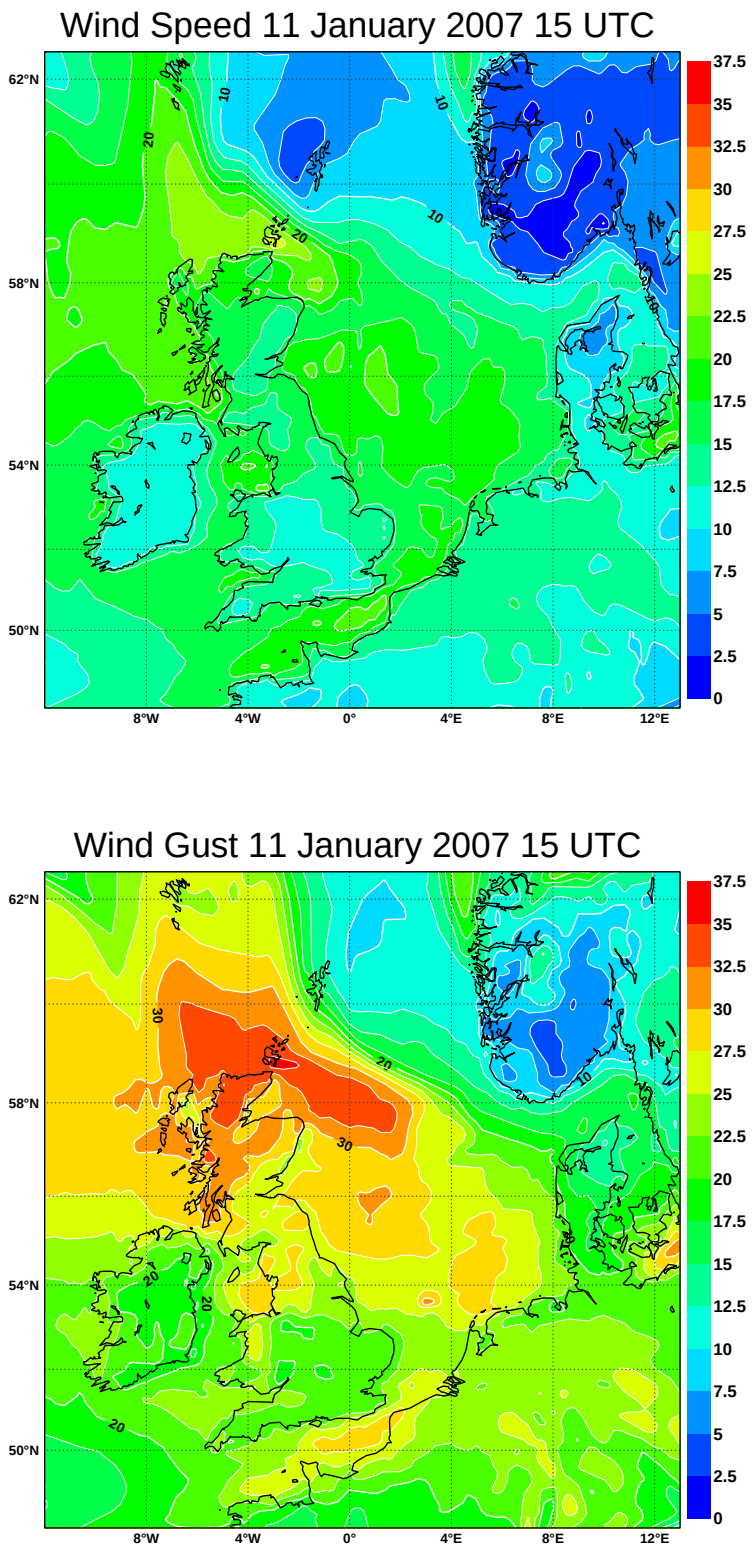

Figure A.2: Contour plot of the wind speed (upper panel) and wind gust (lower panel), in the area of the North Sea. It is an operational forecast of the ECMWF model for 11 January 2007 15 UTC. The wind gust plot is valid from 15 - 18 UTC.

Appendix B

Example of creating spatial correlation

To clarify the method used in section 3.4.1, we consider a simple example, with a very small grid of 4 x 5 grid points. We want to create a wind field, with every grid point influenced by its direct neighbours. To achieve this the matrix $\underline{\underline{\boldsymbol{\nu_u}}}$ in equation (3.3) is not taken the unit matrix anymore. The averaging weights of each neighbour, will be a half of the weight of the value in the grid point itself. So, for the 10^{th} component of $\boldsymbol{u}'$, counted along columns starting from the south east corner, the (unnormalised) weights in the 4 x 5 grid are:

$$w(\hat{i},\hat{j}) = \begin{matrix} 0 & 0 & 0 & 0 & 0 \\ 0 & 0 & \frac{1}{2} & 0 & 0 \\ 0 & \frac{1}{2} & 1 & \frac{1}{2} & 0 \\ 0 & 0 & \frac{1}{2} & 0 & 0 \end{matrix}.$$

The weight values, $\frac{1}{2}$, above and below in the 10^{th} grid point are filled in $\underline{\underline{\boldsymbol{\nu_u}}}$ to the right and left side of the 1's of the unity matrix. The weights, $\frac{1}{2}$, that are on the left and the right of the 10^{th} grid point are different to include. They are situated B further (where B is the amount of grid points along the y-axis), because in the state vector $\boldsymbol{u'}$ neighbouring columns are placed under each other. In this case $B = 4$. So, 4 spaces in the matrix to the left and the right a weight of $\frac{1}{2}$ is filled in. A matrix is created with values for the weights along diagonals, only interrupted due to the borders of the grid.

The total matrix of $\underline{\underline{\boldsymbol{\nu_u}}}$ can be constructed from smaller matrices of B x B dimension. In this example matrix F gives the weights in the vertical line of grid points. Matrix E are the weights one vertical line to the left and the right of the grid point. These weights are symmetrical around the vertical line through the grid point. For this case $\underline{\underline{\boldsymbol{\nu_u}}}$ is

$$F = \begin{pmatrix} 1 & \frac{1}{2} & 0 & 0 \\ \frac{1}{2} & 1 & \frac{1}{2} & 0 \\ 0 & \frac{1}{2} & 1 & \frac{1}{2} \\ 0 & 0 & \frac{1}{2} & 1 \end{pmatrix} \quad E = \begin{pmatrix} \frac{1}{2} & 0 & 0 & 0 \\ 0 & \frac{1}{2} & 0 & 0 \\ 0 & 0 & \frac{1}{2} & 0 \\ 0 & 0 & 0 & \frac{1}{2} \end{pmatrix} \tag{B.1}$$

$$\underline{\underline{\boldsymbol{\nu_u}}} = \gamma \begin{pmatrix} F & E & \dots & \dots & 0 \\ E & F & E & & \vdots \\ \vdots & E & F & E & \vdots \\ \vdots & & E & F & E \\ 0 & \dots & \dots & E & F \end{pmatrix}. \tag{B.2}$$

Now that all the values are created in the matrix with the weights, it has to be multiplied with a factor γ to maintain the same variance in the random wind field. This factor is determined empirically and increases when more neighbours are included.

Appendix C

Notation

Symbols that are used in this study are

AMOUNTG	$H_N - H_T$.
B	number of grid points along the meridional direction.
C	Chézy bottom friction parameter.
C_d	air-sea drag coefficient.
$\mathrm{cov}(u', v')$	covariance between longitudinal and lateral short term wind fluctuations.
$\boldsymbol{D_u}$	N-dimensional state vector with random numbers.
E	submatrix of $\underline{\underline{\boldsymbol{\nu_u}}}$.
ERROR	$H_T - H_O$.
f	Coriolis parameter.
F	submatrix of $\underline{\underline{\boldsymbol{\nu_u}}}$.
f_α	factor that reduces the amount of short term fluctuations.
g	gravitational acceleration.
g	gustiness-constant.
G	wind gust.
H	depth below mean sea level.
h	total depth of fluid. $h = \zeta + H$.
H_N	high and low tide skew surge in the new model.
H_T	high and low tide skew surge in the traditional model.
H_O	high and low tide skew surge of the observations.
i	column of a grid point.
$\hat{i}$	column of a neighbouring grid point.
$\underline{\underline{I}}$	identity matrix.
j	row of a grid point.
$\hat{j}$	row of a neighbouring grid point.
k	number of time steps.
M	maximum of the slowly varying wind in the storm.
n	frequency of short term variations.
N	total number of grid points.
P	the probability that the measured wind gust in a time period T exceeds a value G.
p_a	atmospheric pressure.
r	ratio between $\sigma_{u'}$ and $\sigma_{v'}$.
S_u	spectral density of short term variations.
t	time.
T	period over which wind gust is measured.
t_k	time at a certain time step in the model.
t_s	duration of the storm.

$\boldsymbol{u}$	depth mean velocity.
u	depth mean zonal velocity components of fluid.
U	slowly varying wind speed.
u'	longitudinal velocity component of short term varying wind.
$\boldsymbol{u'}$	N-dimentional state vector with values for longitudinal short term fluctuations.
$\boldsymbol{u_a}$	wind velocity.
$\boldsymbol{u'_a}$	short term varying wind velocity.
$\overline{\boldsymbol{u_a}}$	slowly varying wind velocity
$\boldsymbol{u_{aN}}$	new wind velocity with explicit gustiness.
U_E	slowly varying wind speed in ECMWF model.
$u_\star$	friction velocity.
v	depth mean meridional velocity components of fluid.
v'	lateral velocity component of short term varying wind.
w	weighting factor of the neighbouring grid points.
x	coordinate in the zonal direction.
$\boldsymbol{x}$	location of a grid point.
$\hat{\boldsymbol{x}}$	location of a neighbouring grid point.
x_i	longitude of a grid point.
$x_{\hat{i}}$	longitude of a neighbouring grid point.
y	coordinate in the meridional direction.
y_j	latitude of a grid point.
$y_{\hat{j}}$	latitude of a neighbouring grid point.
z	cooridinate in vertical direction.
α_u	relative amount of longitudinal short term fluctuations.
α_v	relative amount of lateral short term fluctuations.
β	constant that gives the relative impact of gustiness.
β_C	Charnock coefficient.
γ	normalisation constant.
ϵ	constant that gives the relative importance of past deviations.
ζ	sea surface elevation with respect to mean sea level.
κ	Von Karman constant.
$\underline{\underline{\boldsymbol{\nu_u}}}$	$N \times N$ matrix with weights of the neighbouring grid points.
ρ	density water
ρ_a	density air.
$\sigma_{u'}$	gustiness: standard deviation of the longitudinal short term wind fluctuations.
$\sigma_{u',E}$	gustiness in ECMWF model.
$\sigma_{v'}$	standard deviation of the lateral short term wind fluctuations.
$\boldsymbol{\tau_b}$	bottom stress.
τ	characteristic time scale of short term deviations.
τ_{b_x}	zonal component of bottom stress.
τ_{b_y}	meridional component of bottom stress.
$\boldsymbol{\tau_s}$	surface stress.
τ_{s_x}	zonal component of surface stress.
τ_{s_y}	component of surface stress.
ϕ	wind direction.
ϕ_E	wind direction in ECMWF model.

Bibliography

A. C. M. Beljaars. The Influence of Sampling and Filtering on Measured Wind Gusts. *Journal of Atmospheric and Oceanic Technology*, 4:613–626, 1987.

A. C. M. Beljaars, C. Jacob, and J.-J. Morcrette. New physics parameters in the MARS archive. *ECMWF Newsletter*, 90:17–21, 2001.

C.E.P. Brooks and J. Glasspoole. *British Floods and Droughts*. Benn Ltd., London, 1928.

L. Cavaleri and G. J. H. Burgers. Wind gustiness and wave growth. Memorandum OO-92-18, KNMI, 1992.

H. Charnock. Wind stress on a water surface. *Quarterly Journal of the Royal Meteorological Society*, 81: 639–640, 1955.

C. R. Chu, M. B. Parlange, G. G. Katul, and J. D. Albertson. Probability density functions of turbulent velocity and temperature in the atmospheric surface layer. *Water Resources Research*, 32(6):1681–1688, 1996.

M. A. Donelan, F. W. Dobson, S. D. Smith, and R. J. Anderson. On the Dependence of Sea Surface Roughness on Wave Development. *Journal of Physical Oceanography*, 23(9):2143–2149, 1993.

J. R. Garratt. *The Atmospheric Boundary Layer*. Cambridge University Press, Cambridge, 1992.

G. L. Geernaert. *Air-Sea Exchange: Physics, Chemistry And Dynamics*. Kluwer Academic Publishers, Dordrecht, The Netherlands, 1999.

H. Gerritsen, J. W. de Vries, and M. Philippart. The Dutch Continental Shelf Model. In Daniel Lynch and Alan Davies, editors, *Quantitative Skill Assessment for Coastal Ocean Models*, volume 47 of *Coastal and Estuarine Studies*, pages 425–467. American Geophysical Union, 1995.

A.E. Gill. *Atmosphere-ocean dynamics*. Academic Press, 1982.

L.H. Holthuijsen. *Waves in Oceanic and Coastal Waters*. Cambridge University Press, 2007. ISBN 13:978-0-521-86028-4.

K. J. Horsburgh and C. Wilson. Tide-surge interaction and its role in the distribution of surge residuals in the North Sea. *Journal of Geophysical Research.*, 112(C08003), 2007.

J. C. Kaimal, J. C. Wyngaard, Y. Izumi, and O. R. Coté. Spectral characteristics of surface-layer turbulence. *Quarterly Journal of the Royal Meteorological Society*, 98:563–589, 1972.

R. D. Knabb, J. R. Rhome, and D. P. Brown. Tropical Cyclone Report Hurricane Katrina. Report TCR-AL122005, National Hurricane Center, 2005. URL `http://www.nhc.noaa.gov/pdf/TCR-AL122005_Katrina.pdf`.

G. Koopmann. Wasserstandserhöhungen in der Deutschen Bucht infolge von Schwingungen und Schwallerscheinungen und deren Bedeutung bei der Sturmflut vom 16./17. Februar 1962. *Deutsche Hydrographische Zeitschrift*, 15(Heft 5):181–198, 1962.

H. A. Lorentz. Verslag Staatscommissie Zuiderzee 1918 - 1926. Report, Algemene Landsdrukkerij, Den Haag, 1926.

H. Madsen and F. Jakobsen. Cyclone induced storm surge and flood forecasting in the northern Bay of Bengal. *Coastal Engineering*, 51:277 – 296, 2004.

NOAA. Definition wind gust, July 2010. http://www.nws.noaa.gov/forecasts/graphical/definitions/defineWindGust.html.

J. R. A. Onvlee. The performance of drag relations in the WAQUA storm surge model. Technical Reports TR–149, KNMI, 1993.

H. A. Panofsky, H. Tennekes, D. H. Lenschow, and J. C. Wyngaard. The Characteristics of Turbulent Velocity Components in the Surface Layer under Convective Conditions. *Boundary-Layer Meteorology*, 11:355–361, 1977.

M. D. Powell, P. J. Vickery, and T. A. Reinhold. Reduced drag coeficient for high wind speeds in tropical cyclones. *Nature*, 422:279–283, 2003.

S. D. Smith and P. C. P. Chandler. Spectra and gust factors for gale force marine winds. *Boundary-Layer Meteorology*, 40(4):393–406, 1987.

SVSD. Verslag van de stormvloed van 9 november 2007. Report SR88, Ministerie van Verkeer en Waterstaat, 2007. URL http://www.rws.nl/images/SR%2088_tcm174-276325.pdf.

H. Tennekes and J. L. Lumley. *A First Course in Turbulence*. The MIT Press, Cambridge MA, 1972.

UKCP09. UK Climate Projections website, Marine and coastal projections, December 2010. http://ukclimateprojections.defra.gov.uk/content/view/2011/500/.

M. Verlaan, A. Zijderveld, J. W. de Vries, and J. Kroos. Operational storm surge forecasting in the Netherlands: developments in the last decade. *Philosophical Transactions of the Royal Society A*, 363:1441–1453, 6 2005. doi: doi:10.1098/rsta.2005.1578.

T. S. V. Vijaya Kumar, J. Sanjay, B. K. Basu, A. K. Mitra, D. V. Bhaskar Rao, O. P. Sharma, P. K. Pal, and T. N. Krishnamurti. Experimental superensemble forecasts of tropical cyclones over the Bay of Bengal. *Natural Hazards*, 41(3):471–485, 6 2007. doi: doi:10.1007/s11069-006-9055-4. URL http://www.springerlink.com/content/a816377m3212222v.

C. B. Vreugdenhil. *Numerical Methods for Shallow-Water Flow*. Kluwer Academic Publishers, Dordrecht, 1994.

R. H. Weisberg and L. Zheng. Hurricane storm surge simulations comparing three-dimensional with two-dimensional formulations based on an Ivan-like storm over the Tampa Bay, Florida region. *Journal of Geophysical Research*, 113, 12 2008. doi: doi:10.1029/2008JC005115. URL http://dx.doi.org/10.1029/2008JC005115.

B. Wichers Schreur and G. T. Geertsema. Gusto: toepassing van vlaagtheorie op windmetingen en verwachtingen. Scientific Report WR 2006.05, KNMI, 2006. URL http://www.knmi.nl/bibliotheek/knmipubWR/WR2006-05.pdf.

WMO. Definition wind gust, July 2010. http://www.wmo.int/pages/prog/www/DPS/Meetings/ET-EPS-TOKYO/ET-EPS-NEW-Doc3-noeps.pdf.

N. C. Zweers, V. K. Makin, J. W. de Vries, and G. J. H. Burgers. On the influence of changes in the drag relation on surface wind speeds and storm surge forecasts. *Natural Hazards*, Submitted, 2010.